IEEE Access
Multidisciplinary | Rapid Review | Open Access Journal

Received 20 January 2024, accepted 4 February 2024, date of publication 7 February 2024, date of current version 16 February 2024.

Digital Object Identifier 10.1109/ACCESS.2024.3363237

RESEARCH ARTICLE

Optimal Power Flow Incorporating Renewable Energy Sources and FACTS Devices: A Chaos Game Optimization Approach

AMAL AMIN MOHAMED[1], SALAH KAMEL[1], MOHAMED H. HASSAN[2], AND JOSÉ LUIS DOMÍNGUEZ-GARCÍA[3], (Senior Member, IEEE)

[1]Department of Electrical Engineering, Faculty of Engineering, Aswan University, Aswan 81542, Egypt
[2]Ministry of Electricity and Renewable Energy, Cairo 11517, Egypt
[3]IREC Catalonia Institute for Energy Research, Sant Adrià de Besòs, 08930 Barcelona, Spain

Corresponding author: Salah Kamel (skamel@aswu.edu.eg)

This work was supported in part by the European Union's Horizon 2020 Research and Innovation Program under Marie Skł odowska-Curie (Tecniospring Industry) under Grant 801342, and in part by the Government of Catalonia's Agency for Business Competitiveness (ACCIÓ).

ABSTRACT This study addresses the optimal power flow (OPF) problem incorporating renewable energy sources (RES) and flexible alternating current transmission systems (FACTS) using the Chaos Game Optimization (CGO) algorithm. Five objective functions are considered, which include minimizing generation costs, emissions, active power loss, voltage deviation, and enhancing voltage profiles. The OPF formulation considers the anticipated electricity production from wind turbines (WT) and photovoltaic (PV) units as dependent variables, while the voltage magnitude at WT and PV buses is treated as a control variable. Probabilistic models based on wind speed and solar irradiance are used to forecast the electrical output of WT and PV units. The proposed OPF methodology and solution method are validated on the IEEE 30-bus test network. This paper introduces and applies four optimization techniques inspired by biological and natural phenomena, namely CGO, Osprey Optimization Algorithm (OOA), RIME Algorithm, and Slime Mould Algorithm (SMA), to address both single-OPF and multi-OPF objective problems in electric power networks. The suggested optimization approaches are tested under different operational scenarios, considering various combinations of FACTS, renewable energy sources (solar PV and wind), and their locations in the network. To predict wind and solar PV power generation, Weibull and lognormal probability density functions are utilized, respectively. The objective function accounts for reserve cost due to overestimation and penalty cost due to underestimation of intermittent solar and wind power. The results demonstrate that the CGO technique is more efficient than other methods in solving OPF instances.

INDEX TERMS Renewable energy source, wind power generation, solar photovoltaic, FACTS devices, load flow, CGO algorithm.

I. INTRODUCTION

A. BACKGROUND

Presently, incorporating renewable energy sources such as wind turbines and solar photovoltaic systems into the power grid is regarded as a key electrical solution to address the rising demand for electricity caused by population growth and as a means to improve grid efficiency [1]. Furthermore, the escalating global concern for environmental issues and the decreasing costs associated with the implementation and operation of solar and wind power systems have contributed to the growing demand for renewable energy sources. However, the unpredictable nature of renewable energy sources necessitates their consideration when addressing challenges in power dispatch [2]. Recently, an important optimization problem called OPF has been introduced, which

The associate editor coordinating the review of this manuscript and approving it for publication was Hazlie Mokhlis.

deals with both renewable and conventional energy sources. The objective of OPF is to determine the optimal generation and power flow by minimizing a certain objective function, such as electricity losses, production costs, gas emissions, and voltage deviations. Additionally, due to the unstable behavior of renewable energy sources within the power system, managing electrical voltage levels and both reactive and active power injections have become increasingly challenging.

Addressing voltage and reactive power challenges in a dynamic electrical grid can be effectively tackled by leveraging electrical electronic equipment and FACTS devices. These solutions not only promote voltage stability but also offer cost-effective and environmentally friendly power supply options. Both FACTS and OPF operating systems aim to enhance the overall electrical performance of the system [3]. However, previous research on OPF in electrical systems integrated with FACTS has primarily focused on conventional energy sources or employed predetermined profiles for renewable generation (such as wind or PV) without considering their unpredictable behavior. Consequently, resolving OPF issues with a unified objective has been neglected.

This paper aims to address this gap by developing a practical power-flow model for an electrical grid incorporating FACTS, utilizing objective functions that account for the random nature of renewable generation from wind turbines and PV generators. Furthermore, the study will investigate how the placement of FACTS devices and renewable energy sources impacts the efficiency of the electrical system, in contrast to previous studies.

B. LITERATURE REVIEW

In the existing literature, the OPF problem has been addressed with and without the integration of renewable energy sources, employing various optimization techniques. These techniques can be broadly classified into three types: mathematical, heuristic, and metaheuristic approaches. Computational optimization techniques such as linear and quadratic programming, as well as Newton-based methods, have been primarily used to solve single-objective OPF problem. However, computational methods faced challenges when dealing with OPF problems involving multiple objectives, nonlinear functions, or complex issues, especially in contemporary electrical systems with renewable energy sources. Heuristic algorithms offer a simpler approach that does not require extensive reprogramming to accommodate new OPF constraints. References [4], [5] propose alternative optimization techniques to mathematical methods, such as swarm intelligence and support vector machines, within the context of heuristic algorithms. While some studies have explored the benefits of adopting modern optimization algorithms, only a limited number of papers have examined the advantages of employing metaheuristic optimization techniques, which combine mathematical and heuristic approaches.

This optimization strategy employs an approximate optimization technique to tackle challenging issues in OPF, whether renewable energy sources are utilized or not. Various techniques such as Moth Swarm Algorithm (MSO) [4], Grey Wolf Optimization (GWO) [5], hybrid Gradient-Based Optimizer with Moth–Flame Optimization Algorithm (GBO-MFO) [1] are utilized. As mentioned in Section A, FACTS devices play a crucial role in modern electrical systems by reducing power losses, generation costs, and enhancing voltage stability through regulation of transmission line characteristics. However, incorporating FACTS devices in OPF problems increases their complexity and makes optimal solutions more challenging to obtain. The research focuses on solving single-objective OPF problems using heuristic and metaheuristic optimization techniques. For example, Symbiotic Organisms Search (SOS) [6], and TLBO [7] are employed to address OPF problems involving FACTS.

Currently, there is a scarcity of research studies that utilize metaheuristic optimization techniques to solve OPF problems in networks integrated with renewable energy and FACTS devices. Furthermore, no studies have compared novel metaheuristic optimization techniques or examined the impact of renewable energy sources, such as wind and solar, on network efficiency and optimization techniques. However, a recent study conducted by Biswas et al. [8] addressed OPF for the IEEE-30 bus network with the inclusion of wind power and FACTS, utilizing the Success History-based Adaptive Differential Evolution (SHADE) method. However, Biswas et al. did not consider additional OPF issues, such as minimizing voltage deviations, and primarily focused on single and multiple-objective OPF problems related to electricity production costs and power loss. Moreover, Biswas et al. [8] only considered fixed-location wind turbine generators as renewable energy sources, neglecting the inclusion of solar energy units, which are significant contributors to renewable energy production. Our research, on the other hand, takes into account the intermittent behavior of photovoltaic and wind energy generation units, thereby determining suitable placements for FACTS devices and addressing more complex OPF challenges. Previous studies, have mostly resolved OPF issues in electrical networks supported by FACTS without incorporating wind turbine and PV generator units or considering the unpredictable nature of these renewable energy sources. However, our study employs four novel approaches (CGO [9], OOA [10], RIME [11], and SMA [12]) to address challenging OPF and FACTS issues, and their performance is compared with that of conventional optimization techniques. Moreover, the CGO algorithm presents numerous advantages that motivated us to utilize it in solving the OPF problem. It stands out for its simplicity and straightforward implementation. The algorithm's adapted mechanism enables it to avoid suboptimal solutions and ultimately achieve precise estimations

of the optimal solutions. Extensive literature demonstrates the CGO algorithm's ability to effectively enhance initial random solutions and converge towards optimal solutions when applied to various optimization problems. Furthermore, the algorithm's position updating procedure is divided into four distinct stages, each catering to the search space's local and global search requirements with greater sensitivity, resulting in superior outcomes. The objective of this research is to develop innovative metaheuristic optimization methods that enhance the effectiveness of electrical systems by addressing both single and multi-objective AC OPF problems in modern power systems integrated with FACTS devices while considering the unpredictable fluctuations in renewable energy sources. A growing number of photovoltaic (PV) system sectors are utilizing artificial intelligence (AI) as a result of growing computing power, tools, and data creation Power quality will be a key problem as the quickly growing distributed energy resources (DERs) in power networks are now coupled to create community grid architectures. Unless the upstream harmonics are below the thresholds, the grid-to-grid (G2G) bidirectional power transmission among the distribution microgrid will not be deemed financially practicable [13]. It has been discovered that the approaches now in use for a number of solar PV sector tasks connected to design, forecasting, control, and maintenance provide outcomes that are comparatively erroneous. Effective frequency regulation is crucial because of the increasing prevalence of inverter-based renewable energy resources, including photovoltaic (PV) systems, in contemporary power systems, which frequently diminish system inertia and a solar PV system's accurate size is crucial for optimizing the financial life-cycle savings as well as for ensuring the reliability and quality of the power supply [14].

Addressing the optimal power flow challenges becomes increasingly complex when considering the stochastic nature of renewable energy sources in an electrical grid with FACTS devices. Existing approaches in the literature, such as Weibull and lognormal probabilistic estimation methods, are inadequate for accurately modeling and solving the unpredictability of renewable energy sources. To overcome this limitation, this research aims to develop a precise model that effectively addresses the unpredictable nature of renewable energy. In this study, novel meta-heuristic optimization methods, namely CGO, OOA, RIME, and SMA, are employed to mitigate the impact of unpredictable renewable energy sources and FACTS devices on the performance of the electrical network. These methods are specifically crafted to mitigate the impact of unpredictability and optimize OPF objectives, considering both single and multi-objective cost functions. They are compared with alternative algorithms such as the shuffle frog leaping algorithm (SFLA) [15], hybrid SFLA with simulated annealing (SFLA-SA) [16], modified Gaussian bare-bones Levy-flight firefly algorithm (MGBLFA) [16], Gaussian bare-bones Levy-flight firefly algorithm (GBLFA) [16], Levy-flight firefly algorithm (LFA) [16], bare-bones PSO (BBPSO) [16], bare-bones DE (BBDE) [16], PSO [17], artificial bee colony (ABC) [18], grasshopper optimization algorithm (GOA) [19], success history-based adaptive differential evolution using the superiority of feasible solutions (SHADE-SF) [19], grey wolf optimizer (GWO) [20], and PSO [20].

Notably, the novel meta-heuristic optimization algorithms require fewer adjustable parameters compared to existing techniques, simplifying their development and implementation while reducing computational expenses.

C. CONTRIBUTION

This paper is structured around three distinct scenarios to investigate different aspects of optimal power flow (OPF). The first scenario focuses on the base case of OPF without renewable energy in the IEEE-30 bus network. In scenario 1, the study considers OPF in an electrical network where only stochastic wind energy is integrated. Scenario 2 extends the analysis to include both stochastic wind and solar energy in a modified IEEE-30 bus system. Lastly, scenario 3 examines OPF in an electrical network incorporating stochastic wind energy and FACTS devices. Each scenario consists of three cases to provide comprehensive coverage. In the updated IEEE-30 bus system, the availability of wind power is determined using the Weibull probability density function, while solar power is estimated using the lognormal probability density function. Specifically, the thermal units on buses 5, 11, and 13 are replaced with wind generators and solar generators, respectively. However, the intermittent and unpredictable nature of renewable energy sources significantly complicates the OPF analysis when they are incorporated into the system. The paper presents several contributions, which can be summarized as follows:

1) New meta-heuristic optimization methods (CGO, OOA, RIME, and SMA) are developed and utilized to tackle OPF issues, both single and multi-objective, while considering FACTS devices and the unpredictable nature of renewable energy supplies.
2) Unlike previous studies, these research efforts aim to establish an appropriate electrical network framework that integrates the variable power output from renewable generators and the utilization of FACTS devices. Additionally, an evaluation of meta-heuristic optimization techniques addressing electrical grids, with or without FACTS and renewable energy sources, is also included.
3) The effectiveness of the electrical grid is assessed by comparing the performance of these novel meta-heuristic optimization approaches in different scenarios and investigating the impact of renewable energy sources.

D. PAPER OUTLINE

The subsequent sections of the paper are structured as follows: Section II provides a comprehensive description

of the OPF problem, encompassing relevant limitations associated with the issue, as well as the depiction of equality and inequality constraints, FACTS device modeling, and uncertainty modeling for wind and solar power generation. Section III delves into the detailed explanation and application of the CGO algorithm. In Section IV, case studies and simulation results are presented. Finally, Section V encapsulates concluding observations.

II. SUMMARY OF THE OPF PROBLEM

A. MATHEMATICAL EXPRESSION

The primary objective of formulating an OPF problem in an electrical system is to determine the optimal generation mix considering a set of constraints and an objective function. However, OPF problems in electricity networks with FACTS devices and renewable energy sources pose significant challenges due to their nonlinearity and non-convex nature. In this study, we aim to address these objectives for an electrical grid, specifically the 30-bus IEEE system, which is powered by renewable energy sources and equipped with FACTS devices, while accounting for various restrictions including equality and inequality constraints. To incorporate the uncertain nature of renewable energy sources such as photovoltaic (PV) and wind, a probability estimation scheme is developed and presented below. The objectives of the OPF problem are outlined as follows:

1) OBJECTIVE 1: TOTAL COSTS OF GENERATION

Concerning the enhanced system driven by renewable energy sources and furnished with FACTS devices, the overall generation cost encompasses the combined costs of all generation units, including integrated wind turbines and PVs. Due to the variability in the power generated by wind turbines and PVs, the generation cost can be articulated as [23]:

$$\begin{aligned} C_{Total} &= Co_T\left(P_{ThG}\right) + \sum_{y=1}^{N_{wtG}} Co_{wt,y}\left(P_{sc(wt),y}\right) + Co_{Rwt,y} \\ &\times \left(P_{sc(wt),y} - P_{av(wt),y}\right) + Co_{Pwt,y}\left(P_{av(wt),y} - P_{sc(wt),y}\right) \\ &+ \sum_{z=1}^{N_{pvG}} Co_{pv,z}\left(P_{sc(pv),z}\right) + Co_{Rpv,\,z}\left(P_{sc(pv),z} - P_{av(pv),y}\right) \\ &+ Co_{Ppv,z}\left(P_{av(pv),z} - P_{sc(pv),z}\right) \end{aligned} \quad (1)$$

where N_{wtG} and N_{pvG} are the system's total numbers of wind turbines and PVs respectively.

2) OBJECTIVE 2: POWER LOSSES

In the OPF problem, system factors such as voltage deviation and actual power losses play a vital role. It is important to acknowledge that power losses in transmission systems cannot be completely avoided due to the inherent resistance of the lines. The formula for calculating network loss is represented by the range [8]:

$$P_{Loss} = \sum_{m=1}^{nl}\sum_{n=1}^{nl} G_{mn}V^2{}_m + V^2{}_n - 2V_mV_n\,Cos(\rho_{mn}) \quad (2)$$

3) OBJECTIVE 3: GROSS COST

Based on the comparison between the results obtained for Objective 1 and Objective 2 in all cases, it is observed that Objective 2 incurs higher production costs, while Objective 1 leads to higher power losses. This highlights the importance of establishing a goal that takes both factors into consideration, leading us to select Objective 3. To achieve this, a cost model was developed wherein the losses were transformed into an equivalent energy price, allowing for the consideration of both objectives simultaneously. For this investigation, the cost of energy utilized was \$0.10 per kWh. Equation (3) demonstrates that the power cost in this study was \$0.10 per kWh.

$$Gross\ cost = C_{Total} + P_{Loss} * 10^3 * 0.10) \quad (3)$$

B. FACTS DEVICES MODELLING

The primary objective of utilizing flexible AC transmission systems components, such as power electronic converters, is to optimize the efficiency of electrical power transfer and enhance the adaptability and responsiveness of power-flow regulation by manipulating various characteristics of transmission line circuits. In general, a range of FACTS device controllers are developed and deployed to improve the overall effectiveness of the power network. Within this article, two widely used types of FACTS devices, namely shunt controllers (SVC) and series controllers (TCSC and TCPS), are employed. The series controllers (TCSC and TCPS) are placed on the power lines connecting two buses, thereby adjusting the reactance of the power line, which is known as a compensating line. The objective of this process is to enhance the stability of the electrical systems by modifying the line's power-carrying capacity and improving the power flow efficiency of the network.

The role of series controllers (TCSC and TCPS) in FACTS is to regulate the power flow within the electrical network by enabling load increase and reducing line oscillations. This allows for adaptability in the power flow status of the system under different scenarios. On the other hand, the SVC component of FACTS, located at the bus, controls voltages and mitigates fluctuations in power by absorbing or supplying reactive power in the transmission lines. The significance of incorporating FACTS devices into the electrical grid lies in their proper placement, sizing, and coordination. This research has identified the optimal position and size of FACTS devices based on achieving the highest benefits at each cost function.

C. THE LIMITATIONS OF THE ELECTRICITY NETWORK

OPF problems in the power system are subject to several constraints, primarily stemming from physical limitations imposed on the system's hardware and operational parameters such as frequency, current, and voltage. These constraints can be categorized into two main types: equality constraints and inequality constraints.

1) EQUALITY CONSTRAINTS OF OPF

The power balancing equations, characterized by equality constraints, ensure that the active and reactive power generated within the system matches the overall demand while accounting for system losses. This can be mathematically represented as [8]:

$$P_{Gm}-P_{Dm}-V_m\sum_{n=1}^{NB}V_n\gamma_{mn}Cos\left(\partial_{mn}+\rho_m-\rho_n\right)=0\ \forall m\in NB \tag{4}$$

$$Q_{Gm}-Q_{Dm}-V_m\sum_{n=1}^{NB}V_n\gamma_{mn}Cos\left(\partial_{mn}+\rho_m-\rho_n\right)=0\ \forall m\in NB \tag{5}$$

where NB is the overall bus count, P_{Dm} and Q_{Dm} are the active and reactive load requirements at bus m respectively, and $\rho_{mn} = \rho_m - \rho_n$ is the difference in voltage angles between bus m and bus n. The power generating units at bus m P_{Gm} and Q_{Gm}, come from either conventional or renewables, depending on the situation. Between bus m and bus n, respectively, there are two conductances for transfers: G_{mn} and B_{mn}

The power balance while integrating FACTS devices might be described as [23]:

$$P_{Gm}+P_{TCPS\_m}-P_{D\_m}-V_m\sum_{N=1}^{Nb}V_n\gamma_{mn}Cos\left(\partial_{mn}+\rho_m-\rho_n\right)=0 \tag{6}$$

$$Q_{Gm}+Q_{TCPS\_m}-Q_{D\_m}-Q_{SVC\_m}-V_K\sum_{N=1}^{Nb}V_n\gamma_{mn}Sin\left(\partial_{mn}+\rho_m-\rho_n\right)=0 \tag{7}$$

2) INEQUALITY CONSTRAINT OF OPF

a: VOLTAGE DEVIATION

The measurement of the system's voltage stability is assessed through voltage deviation. Voltage deviation is determined by calculating the total deviation of voltages at all load buses (PQ buses) in the system from their nominal value of 1 per unit (p.u.). Mathematically, this can be expressed as:

$$VD=\sum_{p=1}^{NL}\left(\left|V_{Lp}-1\right|\right) \tag{8}$$

b: EMISSIONS

It is common knowledge that producing electricity from traditional energy sources releases hazardous chemicals into the atmosphere. According to the equation in Equation (9), the emission of SOx and NOx rises as the power produced from thermal power plants increases. Calculating emissions in tonnes per hour (t/h) as:

$$Emission,\ E=\sum_{j=1}^{NThG}\left[\left(\alpha_j+\beta_jP_{ThGj}+\gamma_jP^2{}_{ThGj}\right)*0.01+\omega_je^{u_jP_{ThGj}}\right] \tag{9}$$

In which the emission coefficients for the jth thermal generator, α_j, β_j, γ_j, ω_j and u_j, are all present as in [6]. Recent times have seen a significant increase in the pressure placed on the whole energy sector to cut carbon emissions because of global warming [24].

c: POWER GENERATION LIMITATION

The inequality restrictions [25] encompass the operational limitations of the equipment, the components of the electrical network, and the security constraints imposed on lines and loading buses.

$$P_{ThGx}^{min}\le P_{ThGx}\le P_{ThGx}^{max}\quad x=1,\ldots\ldots N_{ThG} \tag{10}$$

$$P_{wt,y}^{min}\le P_{wt,y}\le P_{wt,y}^{max}\quad y=1,\ldots\ldots N_{wt} \tag{11}$$

$$P_{pv,\ z}^{min}\le P_{pv,z}\le P_{pv,z}^{max}\quad z=1,\ldots\ldots N_{pv} \tag{12}$$

$$Q_{ThGx}^{min}\le Q_{ThGx}\le Q_{ThGx}^{max}\quad x=1,\ldots\ldots N_{ThG} \tag{13}$$

$$Q_{wt,y}^{min}\le Q_{wt,y}\le Q_{wt,y}^{max}\quad y=1,\ldots\ldots N_{wt} \tag{14}$$

$$Q_{pv,z}^{min}\le Q_{pv,z}\le Q_{pv,z}^{max}\quad z=1,\ldots\ldots N_{pv} \tag{15}$$

$$V_{Gx}^{min}1\le V_{Gx}\le V_{Gx}^{max}\quad x=1,\ldots\ldots NG \tag{16}$$

Equations (10) - (12) reveal the energy production limitations of thermal technologies, wind generators, and solar PV, respectively. Following the same sequence, Equations (13) - (15) outline the generators' reactive power capacity. Equation (16) details the voltage restrictions imposed on generator buses.

d: SECURITY CONSTRAINT

$$V_{L_p}^{min}\le V_{L_p}\le V_{L_p}^{max}\quad P=1,\ldots\ldots NL \tag{17}$$

D. MATHEMATICAL SIMULATIONS FOR RENEWABLE ENERGY SOURCES

In recent years, power markets and networks have been significantly impacted by renewable energy sources [1]. Therefore, incorporating renewable energy sources into electric network structures is crucial to enhance the dependability and quality of systems [1]. Renewable energy sources, being inherently unpredictable and influenced by weather conditions, pose challenges in accurately predicting their supply and optimizing the optimal power flow (OPF)

issue. Consequently, successfully addressing the OPF for electrical systems with renewable energy sources necessitates a probability prediction scheme for their characteristics, rather than relying on accurate characteristics or predictable forecast profiles.

To effectively address the OPF issue, a probabilistic forecasting model is proposed to cope with the uncertainty in renewable energy supply profiles. The study focuses on the IEEE 30-bus electrical system, incorporating wind and solar energy sources under various geographical scenarios. Probabilistic techniques, specifically Weibull and lognormal distributions, are employed to calculate the wind and solar energy production [23]. In the electrical system model, the profiles of wind and photovoltaic (PV) production are considered as negative load values, prioritizing the utilization of available renewable energy resources before relying on the remaining thermal generating sources. Consequently, this approach leads to a reduction in overall load demand, generating costs, and electricity loss from the thermal units [2].

• *Cost Estimation for Thermal Power Plants:*

The operation of thermal generators necessitates the use of fossil fuels. The quadratic relationship provides a description of the correlation between the fuel costs ($/h) and the generated output (MW):

$$Co_{Th0}\,(P_{ThG}) = \sum_{x=1}^{N_{ThG}} a_x \quad + b_x P_{ThGx} + C_x\, P^2{}_{ThGx} \qquad (18)$$

In which the cost coefficients for the x^{th} thermal generator that generates output power P_{ThGx} are a_x, b_x, and C_x. N_{ThG} is the maximum number of generating units. For a more realistic and accurate cost function modeling, the valve-point impact must be taken into account. There is more fluctuation in the fuel-cost relations in the thermal producing units with multi-valve turbine generators [2]. In order to add its exact value to the fundamental cost function in Equation, the valve loading impact of multi-valve steam turbines is treated as a sinusoidal function (18). The following is the total cost ($/h) of thermal unit output:

$$Co_{Th}\,(P_{ThG}) = \sum_{x=1}^{NThG} a_x \quad + b_x P_{ThGx} + C_x \;\; P^2{}_{ThGx} + \left| d_x \quad \times \sin(e_x \quad \times (\, P^{Min}_{ThGx} - P_{ThGx})) \right| \qquad (19)$$

In which the valve-point loading affect coefficients d_x and e_x are shown. The least power that the x^{th} thermal units can produce while it is operating is known as P^{Min}_{ThGx}.

• *Direct Cost of Wind and Solar Cost of Wind and Solar Photovolatic Power:*

Unlike traditional thermal power plants, solar photovoltaic and wind power producers do not require fuel. This absence of fuel cost may result in the omission of a cost function, particularly if the wind and solar photovoltaic facilities are owned by the independent system operator (ISO) [23]. Since these facilities do not incur fuel costs, the ISO may choose to allocate expenses for repairs, replacements, or the initial investment in the wind and solar photovoltaic installations. However, when wind or solar photovoltaic facilities are owned by private parties, the ISO pays a price based on the contractually agreed-upon planned electricity. In this case, a function of planned power is used to represent the direct costs associated with wind turbine power from the y^{th} plant.

$$Co_{wt\_y}(P_{sc(wt)\_y}) = g_y(P_{sc(wt)\_y}) \qquad (20)$$

where $P_{sc(wt)\_y}$ is the scheduled power from the y^{th} wind power station, and g_y is its direct cost coefficient. Similarly, to wind power plants, the k^{th} solar PV plant's direct cost is:

$$Co_{pv\_Z}(P_{sc(pv)\_Z}) = g_r(P_{sc(pv)\_Z}) \qquad (21)$$

If g_r represents the direct cost factor for the Z^{th} solar PV plant, the scheduled power for the same plant is $P_{sc(pv)\_Z}$

• *Cost Analysis of Wind Power Uncertainty:*

The potential issue of generating less electricity than anticipated by the wind farm is commonly referred to as overestimating the power from an unknown source. To maintain a reliable power supply for customers, the system operator must allocate spinning reserves to account for such situations. The cost incurred by using reserve-producing units to compensate for the overestimated demand is known as the reserve cost [8].

Reserve cost is determined as follows for the jth wind turbine plant

$$\begin{aligned} &Co_{Rwt,\,y}\left(P_{sc(wt),y} - P_{av(wt),y}\right) \\ &\quad = U_{Rwt,y}\left(P_{sc(wt),y} - P_{av(wt)_y}\right) \\ &\quad = U_{Rwt,y}\int_0^{P_{sc,y}} \left(P_{sc(wt),y} - P_{wt,y}\right) f_{wt} P_{wt,y})\mathrm{d}p_{wt,y} \end{aligned} \qquad (22)$$

where $P_{av(wt),y}$ is the actual power produced by the same wind farm, and $u_{Rwt,y}$ is the reserve cost factor for the y^{th} wind power plant. The wind energy probability density function for the $y^{th}-$ wind farm is given by $f_{wt}P_{wt,y}$. In contrast to the overestimation scenario, there can be instances in the system where the wind farm generates more electricity than initially anticipated. This situation leads to the undervaluation of renewable energy production. If it is not possible to utilize the surplus electricity by reducing the output of traditional generators, it will go to waste. In such cases, the ISO incurs a penalty fee for the excess amount that was generated.

For the y^{th} wind energy station, the penalty cost is described as follows**:**

$$\begin{aligned} &Co_{pwt,\,y}\left(P_{av(wt),y} - P_{sc(wt),y}\right) \\ &\quad = U_{pwt,y}\left(P_{av(wt),y} - P_{sc(wt),y}\right) \\ &\quad = U_{pwt,y}\int_{P_{sc,y}}^{P_{wtr,y}} \left(P_{wt,y} - P_{sc(wt),y}\right) f_{wt} P_{wt,y})\mathrm{d}p_{wt,y} \end{aligned} \qquad (23)$$

where $u_{pwt,y}$ is the penalty cost factor for the y^{th} wind turbine and $P_{wt,y}$ is the wind turbine's rated output produced power.

• *Cost Analysis of Solar of Photovolatic Power Uncertainty:*

Solar PV plants, similar to wind turbines, generate energy sporadically and with uncertainty. Consequently, the approach for over- and underestimating solar power should theoretically be analogous to that used for wind power. Moreover, it is worth noting that solar radiation is commonly modeled as lognormal [26]. In contrast to wind distributions, which are typically described by the Weibull probability density function (PDF), the models for reserve and penalty costs are formulated based on the concept presented in [26] to facilitate calculations. The reserve cost for the solar PV plant is as follows:

$$\begin{aligned} &Co_{Rpv,\,Z}\left(P_{sc(pv),Z}-P_{av(pv),Z}\right)\\ &\quad=U_{Rpv,M}\left(P_{sc(pv),Z}-P_{av(pv),Z}\right)\\ &\quad=U_{Rpv,Z}{*}f_{pv}\left(\left(P_{av(pv),Z}\right.\right.\\ &\quad\left.\left.<P_{sc(pv),Z}\right)\right){*}\left[P_{sc(pv),Z}\right.\\ &\quad\left.-E\left(P_{av(pv),Z}<P_{sc(pv),Z}\right)\right] \end{aligned} \tag{24}$$

where $Co_{Rpv,\,Z}$ is the reserve cost factor for the zth solar PV plant and $P_{av(pv),y}$ is the actual amount of electricity the plant has available. The likelihood that solar power will be in short supply compared to the planned power $P_{sc(pv),y}$ is given by the formula $f_{pv}\left(\left(P_{av(pv),Z}<P_{sc(pv),Z}\right)\right)$, and the expected solar PV power is given by the formula $E\left(P_{av(pv),Z}<P_{sc(pv),Z}\right)$, The solar PV plant's penalty cost is the following:

$$\begin{aligned} &Co_{Ppv,\,Z}\left(P_{av(pv),Z}-P_{sc(pv),Z}\right)\\ &\quad=U_{Ppv,Z}\left(P_{av(pv),Z}-P_{sc(pv),Z}\right)\\ &\quad=U_{Ppv,Z}{*}f_{Ppv}\left(\left(P_{av(pv),Z}>P_{sc(pv),Z}\right)\right)\\ &\quad{*}\left[E\left(P_{av(pv),Z}>P_{sc(pv),Z}\right)-P_{sc(pv),Z}\right] \end{aligned} \tag{25}$$

where $P_{av(pv),Z}>P_{sc(pv),Z}$ is the likelihood of solar energy excess than the planned power ($P_{sc(pv),Z}$), and E ($P_{av(pv),Z}>P_{sc(pv),Z}$) is the anticipation of solar PV power beyond $P_{sc(pv),Z}$

E. MODELS FOR UNCERTAINTY AND STOCHASTIC WIND AND SOLAR POWER

The distribution of wind speeds is widely recognized to conform to the Weibull probability density function (PDF) [1]. When applying the Weibull PDF with shape factor (h) and scale factor (s), the probability of a wind speed v in meters per second (m/s) can be expressed as follows:

$$f_v(v)=\left(\frac{h}{s}\right)\left(\frac{v}{s}\right)^{(h-1)}e^{\left(-\frac{v}{s}\right)^k}\quad for\;\;0<v<\infty \tag{26}$$

In our study of the IEEE-30 bus network, the traditional generators in buses 5 and 11 have been replaced with wind generators. The chosen Weibull shape (h) and scale (s) values are provided in Table 1. Throughout the study, we adhere to these specified Weibull probability density function (PDF) parameters, unless stated otherwise for a particular case study. After conducting 8000 Monte-Carlo simulations, we generated the Weibull fitting and wind frequency distributions, which are depicted in Figures 1 and 2, respectively. The design requirements for wind turbines are outlined in Standard [28], which also specifies the highest turbulence class IA for turbines approved to operate at a maximum annual average wind speed of 10 m/s at hub height. Moreover, the various PDF parameter values for the two wind farms reflect the genuine geographical diversity of their respective locations. Solar photovoltaic unit has been installed in place of the traditional generator at bus 13. The unit's production is based on the solar irradiance (si) that follows lognormal PDF [26]. When solar irradiance (si) follows a lognormal PDF with mean u and standard deviation α, the probability is:

$$f_G\,(\mathrm{si})=\frac{1}{si\alpha\sqrt{2\pi}}exp\left\{\frac{\left((\ln L-u)^2\right)}{2\alpha^2}\right\}\quad \text{for si}>0 \tag{27}$$

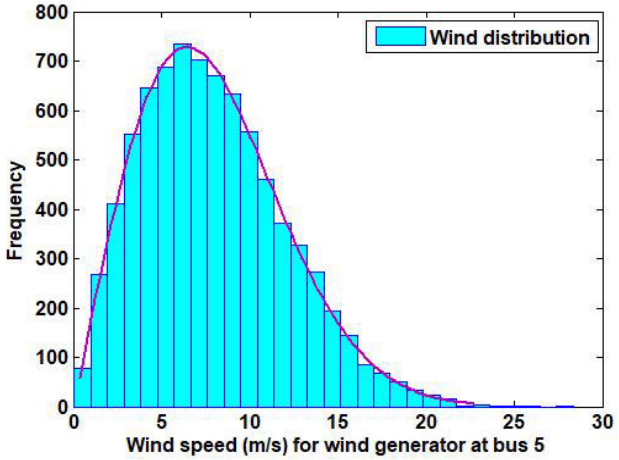

FIGURE 1. Distribution of wind speeds at the wind farm at bus 5 (s = 9, h = 2).

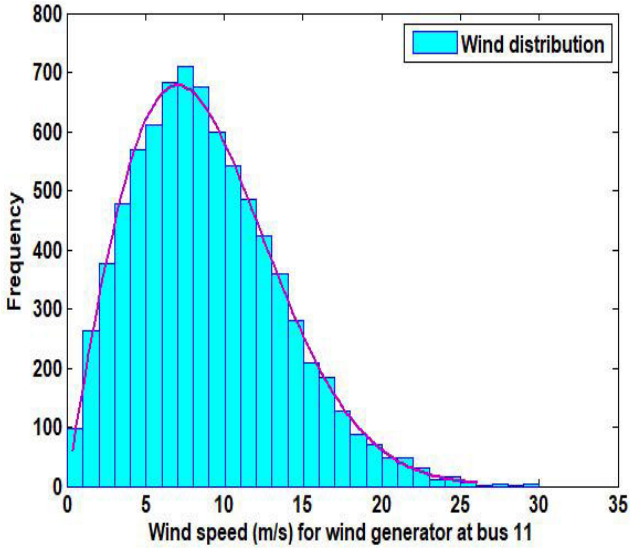

FIGURE 2. Distribution of wind speeds for wind farm at bus 11 (s = 10, h = 2).

Figure 3 presents the frequency distribution and lognormal fitting of solar irradiance, obtained through an 8000-sample Monte Carlo simulation. The specific parameters for the lognormal probability density function (PDF) are listed in Table 1. Throughout the study, we maintain adherence to these PDF specifications, unless otherwise specified for a specific case.

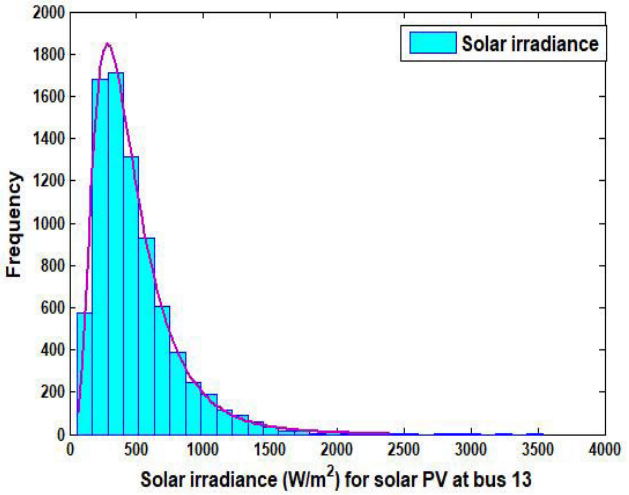

FIGURE 3. Distribution of solar irradiation for PV at bus 13.

• *A Model for Wind and Solar Photovolatic Power:*

The collective power generated by the 25 wind turbines in the farm is assumed to be connected to bus 5, while the production from the wind farm with 20 turbines is connected to bus 11. Each individual turbine has a maximum output capacity of 3 MW. The actual power produced by a wind turbine varies depending on the wind speed it encounters. The relationship between wind speed (v) and the produced power of a turbine can be described as follows:

$$P_{wt}(\mathrm{v}) = \begin{cases} 0 & for\ v < v_{in}\ and\ v > v_{out} \\ P_{wtr}\left(\dfrac{v - v_{in}}{v_r - v_{in}}\right) & v_{in} \le v \le v_{rated} \\ P_{wtr} & for\ v_{rated} \le v \le v_{out} \end{cases} \tag{28}$$

where v_{in}, v_{out} and v_{rated} represent the turbine's cut-in, rated, and cut-out wind speeds, respectively, the rated produced power of the wind turbine is represented by P_{wtr}. v_{in}= 14 m/s, v_r=16 m/s, and v_{out} =25 m/s are the different speed numbers.

According to [23], solar PV converts solar irradiance (si) to electricity as follows:

$$P_{pv}(\mathrm{si}) = \begin{cases} p_{pvr}\left(\dfrac{si^2}{si_{std} R_{ci}}\right) & for\ 0 < si < R_{ci} \\ p_{pvr}\left(\dfrac{si}{si_{std}}\right) & for\ si \ge R_{ci} \end{cases} \tag{29}$$

where, si_{std} is the typical environment's solar irradiance, which is set at 800 W/m2. The irradiance point R_{ci} has a value of 120 W/m 2.p_{pvr}: Stands for the rated generated power of solar PV

• *Probability Calculations for Wind Power:*

It can be seen from Equation. (28), that the fluctuating wind power is discontinuous in a few wind speed zones. Power production is 0 when wind speed v_{in} is less than cut-in speed (vin) and greater than cut-out speed (v_{out}). The wind turbine produces rated power P_{wtr} between rated wind speed (v_{rated}) and cut-out speed (v_{out}). Ref. [2] gives the probability for these separate zones:

$$f_{wt}(P_{wt})\{(P_{wt} = 0\} = 1 - exp\left[-\left(\frac{v_{in}}{\beta}\right)^{(\gamma)}\right] + exp\left[-\left(\frac{v_{out}}{\beta}\right)^{(\gamma)}\right] \tag{30}$$

$$f_{wt}(P_{wt})\{(P_{wt} = P_{wtr}\} = exp\left[-\left(\frac{v_{rated}}{\beta}\right)^{(\gamma)}\right] - exp\left[-\left(\frac{v_{out}}{\beta}\right)^{(\gamma)}\right] \tag{31}$$

The continuous region's probability is computed as [57]:

$$f_{wt}(p_{wt}) = \frac{k(v_{rated} - v_n)}{s^h * p_{wtr}}\left[v_{in} + \frac{p_{wt}}{p_{wtr}}(v_{rated} - v_{in})\right]^{h-1} \times exp\left[-\left(\frac{v_{in} + \frac{p_{wt}}{p_{wtr}}(v_{rated} - v_{in})}{s}\right)^{h}\right] \tag{32}$$

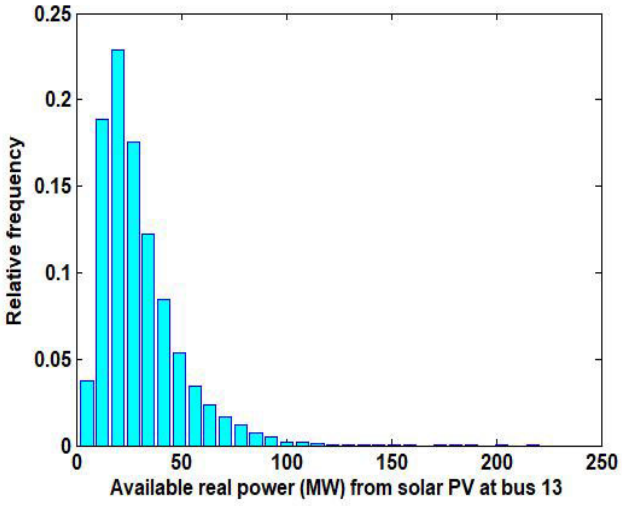

FIGURE 4. Actual PV power distribution at bus 13 in MW.

• *Computation of Solar Power Over L Under Estimate Costs:*

The distribution of solar irradiation for PV at bus 13 and stochastic energy production from the solar PV system is represented by the histograms in Figures 3 and 4. The scheduled electricity delivery from the solar PV system to the grid is indicated by the magenta dotted line. As mentioned earlier, the scheduled power can be any agreed-upon amount

TABLE 1. The parameters of wind turbine generating units and solar PV plants.

Wind turbine generating units [8]					Solar PV plant [23]		
Wind farm	No. of turbines	Power rating (P_{wtr})	Parameters for Weibull PDF	Weibull mean, M_{wbl}	Power rating (P_{pvr})	Parameters of Lognormal PDF	Lognormal mean, M_{LGN}
1@ bus 5	25	75	s= 9, h=2	v = 7.976 m/s	50@ bus 13	$\alpha = 0.6$	$si = 483\ w/m2$
2@ bus 11	20	60	s=10, h=2	v = 8.862 m/s		$u = 6$	

of electricity between the ISO and the owners of the solar PV system. The cost associated with overestimation can be expressed as follows:

$$C_{Rs}\,(P_{ss}-P_{sav}) = K_{Rs}\,(P_{ss}-P_{sav}) = K_{Rs}\sum_{n=1}^{N^-}\left[P_{ss}-P_{sn_-}\right]*f_{sn_-} \tag{33}$$

where P_{sn_-}, on the left-half plane of P_{ss} in the histogram, is the accessible power that is lower than the scheduled power P_{ss}. The relative frequency with which P_{sn_-} occurs is denoted by f_{sn_-}. N^- is the quantity of discrete bins on the left-hand side of P_{ss}, or, alternatively, the quantity of pairs (P_{sn_-}; f_{sn_-}) produced for the PDF, Results validity is somewhat improved by using more segments.

Similar calculations may be made for the underestimating cost as:

$$C_{ps}\,(P_{sav}-P_{ss}) = K_{Ps}\,(P_{sav}-P_{ss}) = K_{ps}\sum_{n=1}^{N^+}\left[P_{sn_+}-P_{ss}\right]*f_{sn_+} \tag{34}$$

where P_{sn_+}, on the right-half plane of Pss in the histogram, is the accessible power greater than the schedule power P_{ss}. The relative frequency at which P_{sn_+} occurs is given by f_{sn_+}. N is the quantity of discrete bins on the right-hand side of P_{ss}, or, alternatively, the quantity of pairs (P_{sn_+}; f_{sn_+}) produced for the PDF.

III. METAHEURISTIC OPTIMIZATION ALGORITHMS

A. CHAOS GAME OPTIMIZATION ALGORITHM

This paper employs and adapts recently developed meta-heuristic optimization techniques, namely CGO, OOA, RIME, and SMA, to tackle optimal power flow (OPF) challenges and effectively handle the inherent uncertainty introduced by the integration of renewable energy sources into the electrical grid. These novel meta-heuristic optimization algorithms offer potential solutions for resolving complex power-flow issues, both in terms of single and multiple-objective functions, in an electrical grid interconnected with stochastic renewable energy sources and FACTS devices.

Considering the significant benefits associated with reducing emissions, minimizing electricity losses, and optimizing generating costs, the development of appropriate and innovative optimization models for electrical network applications holds global importance. The proposed novel meta-heuristic optimization strategies are specifically designed to address stochastic, volatile, and challenging optimization problems that arise in such contexts. The utilization of the CGO algorithm is supported by multiple factors. Firstly, in the original paper, a comparative analysis with other equipped algorithms (FA, GWO, ICA, SOS, TLBO, and the WOA) reveals that the CGO algorithm consistently yields highly satisfactory results when handling test functions of varying dimensions. This is evidenced by the comparative results obtained from the CEC 2017 competition's test functions. Additionally, considering all the 2D, 50D, and 100D test functions, a comprehensive comparison indicates that the CGO algorithm consistently outperforms other metaheuristics, making it the optimal choice in every scenario. Moreover, the CGO algorithm exhibits superior performance in achieving the global bests of mathematical functions, surpassing other metaheuristics, depending on the chosen tolerance.

1) INSPIRATION

The mathematical aspect of chaos theory examines the unique characteristics of system dynamics that exhibit high sensitivity to their initial conditions. Chaos theory elucidates how the dependence of a dynamical system on its starting conditions can result in even minor variations in those conditions leading to profound impacts on the system's future states.

2) MATHEMATICAL MODEL

This study explores an optimization technique based on the principles of chaos theory. The simulation theorem for the CGO algorithm is developed by incorporating the fundamental concepts of the chaos game and fractals. In the CGO method, multiple response possibilities (M) are considered, which represent eligible seeds within a Sierpinski triangle. This is because many natural evolution techniques maintain a population of potential solutions that undergo random changes and selection.

In this technique, each potential solution (candidate) (M_i) consists of decision variables that indicate the location of

eligible seeds within the Sierpinski triangle. The Sierpinski triangle is considered the search space for potential solutions in the metaheuristic approach. These mathematical aspects are presented as follows:

$$M = \begin{bmatrix} M_1 \\ M_2 \\ \vdots \\ M_i \\ \vdots \\ M_n \end{bmatrix} = \begin{bmatrix} M_1^1 & M_1^2 & \cdots & M_1^j & \cdots & M_1^d \\ M_2^1 & M_2^2 & \cdots & M_2^j & \cdots & M_2^d \\ \vdots & \ddots & \vdots & \vdots & \ddots & \vdots \\ M_i^1 & M_i^2 & \cdots & M_i^j & \cdots & M_i^d \\ \vdots & \ddots & \vdots & \vdots & \ddots & \vdots \\ M_n^1 & M_n^2 & \cdots & M_n^j & \cdots & M_n^d \end{bmatrix}, \quad \begin{cases} i = 1, 2, \ldots n \\ i = 1, 2, \ldots .d \end{cases} \tag{35}$$

where n is the total number of eligible seeds and d is their dimensions. The following beginning places of these viable seeds are chosen at random in the problem space:

$$M_i^j(0) = M_{i,min}^j + rand.\left(M_{i,max}^j - M_{i,min}^j\right) \quad \begin{cases} i = 1, 2, \ldots n \\ i = 1, 2, \ldots .d \end{cases} \tag{36}$$

where $M_i^j(0)$ establishes the starting placement of the eligible seeds, $M_{i,min}^j$ and $M_{i,max}^j$ are the minimum and maximum permitted values for the jth decision variable of the ith solution candidate, respectively; The range [1, 0] is the range of a random number called rand. Additionally, the approach of planting new seeds within a Sierpinski triangle is used. A temporary triangle having three seeds is created for each of the viable seeds in the solution space (M_i) as described in the following:

- The currently discovered Global Best position (GB)
- The location of the Mean Group (MG_i)
- The placement of the chosen seed (M_i)

The first seed is shown mathematically as:

$$Sead_i^1 = M_i + \sigma_i * (\delta_i * GB - \gamma_i * MG_i)\, i = 1, 2, ..n \tag{37}$$

The second seed is shown mathematically as:

$$Sead_i^2 = GB + \sigma_i * (\delta_i * M_i - \gamma_i * MG_i)\, i = 1, 2, ..n \tag{38}$$

It deserves to be mentioned that the seed can also be moved in the direction of the linked lines connecting the M_i and the GB. For this, a few random factorials are also employed as follows:

$$Sead_i^3 = MG_i + \sigma_i * (\delta_i * M_i - \gamma_i * GB_i)\, i = 1, 2, ..n \tag{39}$$

The fourth seed is shown mathematically as:

$$Sead_i^4 = M_i(M_i^k + M_i^k + R) \quad k = 1, 2, ..d \tag{40}$$

IV. SIMULATION RESULTS TO THE TEST SYSTEM FOR OPF SOLUTIONS

In order to assess and validate the effectiveness of the proposed novel metaheuristic optimization algorithms, renewable energy sources and FACTS devices were implemented on an IEEE 30-bus system. The system comprises 41 transmission lines, with four transformers having non-standard tap ratios at lines 6-9, 6-10, 4-12, and 28-27. There are also six thermal generators located at buses 1, 2, 5, 8, 11, and 13. The boundaries for generator voltages and transformer tap settings are defined as (0.9, 1.1) p.u. and (0.95, 1.1) p.u., respectively. The voltage at the load buses is constrained between 0.95 and 1.05 p.u., as detailed in Table 2. The relevant information and operational conditions of the test system are thoroughly examined in [29].

In this study, the proposed method is implemented and improved using MATLAB 2014, a programming environment. The simulation models for the suggested metaheuristic optimization techniques were developed using a 2.8 GHz i3 CPU with 4 GB of RAM. The power flow evaluation was conducted using MATPOWER version 7 [30]. A total of nine different test cases were considered, as outlined in Table 3. The results from the case studies, which employed various metaheuristic approaches, are compiled and presented in this section. To validate the reliability of the results, a comparison was made with other methods mentioned in this study. Subsequently, the proposed technique was employed to investigate the impact on the total operating expenses of the system when PV and wind generators were incorporated

A. BASE CASE

In this particular scenario, the proposed method was utilized to solve the conventional OPF problem with a fixed load. To validate its performance, the results obtained from the suggested approach were compared to those obtained from OOA [10], RIME [11], and SMA [12]. Additionally, comparisons were made with techniques mentioned in other papers, namely SFLA [15], SFLA-SA [16], MGBLFA [16], GBLFA [16], LFA [16], BBPSO [16], BBDE [16], and PSO [17]. The objective was to minimize the cost of the thermal generator without incorporating any renewable energy sources. The population sizes were set at 100 for all four algorithms, with a maximum of 300 iterations. The outcomes from different algorithms were compared with the objective function in Table 4. The CGO algorithm demonstrated superior performance, achieving a generation cost of 832.0665 $/h, outperforming all other algorithms. A comparison of the convergence curves of the objective function for the various strategies is presented in Figure 5, highlighting the CGO algorithm's ability to achieve the lowest cost with fewer iterations than other approaches.

B. WIND ELECTRICAL NETWORK

In this case, the optimal power flow (OPF) problem is addressed by incorporating renewable energy sources

TABLE 2. Analysis of the IEEE-30 bus system.

Details	Quantity	Item
[29]	30	No. of buses
[29]	41	No. of branches
Buses; 1 (Slack), 2, and 8	3	Thermal generators (Thg)
Buses; 5 and 11	2	Wind generators (WT)
Bus 13	1	PV units (PV)
Branch positioning and rating improved	2	TCSC
Branch positioning and rating improved	2	TCPS
Branch positioning and rating improved	2	SVC
Branches; 11, 12, 15 and 36	4	Tap changing transformer
Scheduled actual power for 5 No. generators, including: Thg2, Thg3, WT1, WT2 and PV1	5	Control variables
The generator buses' bus voltages	6	
283.4 MW, 126.2 MVAr	-	Attached load
[0.95–1.05] p.u.	24	Permitted range of load bus voltage

TABLE 3. An overview of the case studies for the modified IEEE-30 bus test system.

Case	Objective function		System description	Table
Base case	Minimization fuel cost	Obj 1	System with out renewable sources or FACTS devices	Table 4
Case 1	Minimization generation cost	Obj 1	System with two wind turbine	Table 5
Case 2	Minimization power loss	Obj 2	System with two wind turbine	Table 6
Case 3	Minimization gross cost	Obj 3	System with two wind turbine	Table 7
Case 4	Minimization generation cost	Obj 1	System with two wind turbine and one PV	Table 8
Case 5	Minimization power loss	Obj 2	System with two wind turbine and one PV	Table 9
Case 6	Minimization gross cost	Obj 3	System with two wind turbine and one PV	Table 10
Case 7	Minimization generation cost	Obj 1	System with two wind turbine and six FACTS devices	Table 11
Case 8	Minimization power loss	Obj 2	System with two wind turbine and six FACTS devices	Table 12
Case 9	Minimization gross cost	Obj 3	System with two wind turbine and six FACTS devices	Table 13

TABLE 4. Comparison of the cgo technique's results with those of alternative fuel cost reduction function optimization approaches for base case.

Technique	Emission (t/h	Fuel Cost ($/h)	V.D. (p.u.)	Power Losses (MW)
CGO	0.3194	832.0665	0.8581	10.6311
OOA	0.287	850.549	0.5511	8.5727
RIME	0.3195	832.799816	0.3528	10.7817
SMA	0.3196	832.3042	0.8414	10.7848
SFLA [15]	-	834.8166	-	-
SFLA-SA [16]	-	834.6339	-	-
MGBLFA [16]	0.4381	832.1713	0.8697	10.70
GBLFA [16]	0.4379	832.3921	0.8859	10.6895
LFA [16]	0.4427	832.3806	0.8734	10.7268
BBPSO [16]	0.4400	832.6437	0.8813	10.7091
BBDE [16]	0.4341	832.2945	0.8846	10.7148
PSO [17]	-	832.6871	-	-

TABLE 5. Optimum control variables and objective function values for case 1.

TABLE 5. OPTIMUM CONTROL VARIABLES AND OBJECTIVE FUNCTION VALUES FOR CASE 1

Control Variable	Minimum	Maximum	CGO	OOA	RIME	SMA
$P_{Thg\,2}$(MW)	20	80	40.65310	39.2788	43.8114	42.06893
$P_{WT\,5}$(MW)	0	75	49.834900	46.909	49.59553	48.810142
$P_{Thg\ 8}$(MW)	10	35	10.0000	12.433	10.0735	10.00
P_{WT11}(MW)	0	60	41.780940	38.884	39.0323	41.432
$P_{Thg\,13}$(MW)	12	40	12.0000	17.2881	12.0184	12.0004
V_1(p. u)	0.95	1.10	1.0733676	1.0733	1.0782	1.0772
V_2(p. u)	0.95	1.10	1.058717	1.0426	1.06530	1.0600
V_5(p. u)	0.95	1.10	1.036867	1.0148	1.0393	1.0394
V_8(p. u)	0.95	1.10	1.03771	1.0267	1.03623	1.0403
V_{11}(p. u)	0.95	1.10	1.094572	1.0724	0.99635	1.1
V_{13}(p. u)	0.95	1.10	1.0828142	0.9937	1.06207	1.0685
T_{11}(p. u)	0.90	1.10	1.04999	1.0049	1.011698	1.0142
T_{12}(p. u)	0.90	1.10	0.908422	0.97174	0.91370	0.900
T_{15}(p. u)	0.90	1.10	1.029993	1.07287	1.04529	1.0039
T_{36}(p. u)	0.90	1.10	0.951453	0.979273	0.97487	0.95369
P_{Slack}	50	200	134.9079	35.8921	134.9495	134.9134
$Q_{Thg\,1}$(MVAr)	-20	150	0. 92	-7.18	1.13	7.94
$Q_{Thg\,2}$(MVAr)	-20	60	17.32	5.45	33.92	13.73
Q_{WT5}(MVAr)	-30	35	25.1	29.33	26.78	27.12
$Q_{Thg\,8}$(MVAr)	-15	48.7	37.03	43.24	46.71	43.1
$Q_{WT\ 11}$(MVAr)	-25	30	29.99	17.38	-1.38	28.05
$Q_{Thg\,13}$(MVAr)	-15	44.7	30.37	29.79	32.9	19.2
C_{gen}($/h)			807.88474	813.9549	809.005	807.9107
P_{loss}(Mw)			5.7769	6.2967	6.0809	5.8254
C_{gross}($/h)			1385.6	1443.6	1417.1	1390.4
VD(p. u.)			0.6585	0.7081	0.3825	0.7224
Emission			0.2135	0.2110	0.2134	0.2134

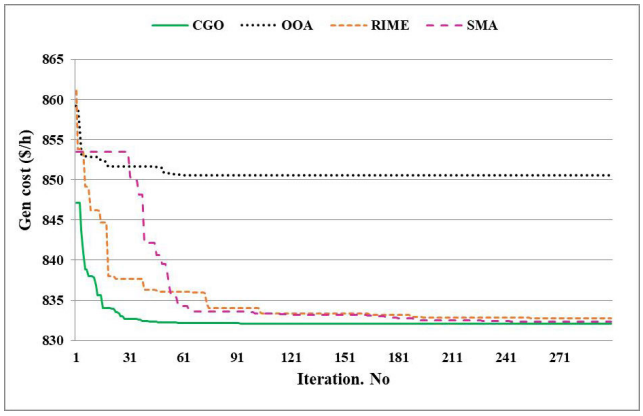

FIGURE 5. Comparison of OPF convergence curves (Base Case).

(specifically wind turbines) while considering factors such as generation cost, power loss, and voltage profile improvement. As the wind speed increases, the wind generation system produces more energy, resulting in reduced overall operation costs. Moreover, the thermal generators in the power system possess surplus up/down spinning reserve capacity compared to the system's total up and down spinning reserve demand. Consequently, a portion of the load is fulfilled by the wind generators, thereby affecting the load on thermal generators, altering the flow of transmission lines, and subsequently impacting the transmission losses in the power system. The obtained results are then compared with those of CGO, RIME, OOA, and SMA techniques. The findings of this case study for all the mentioned techniques are summarized in Tables 5-7.

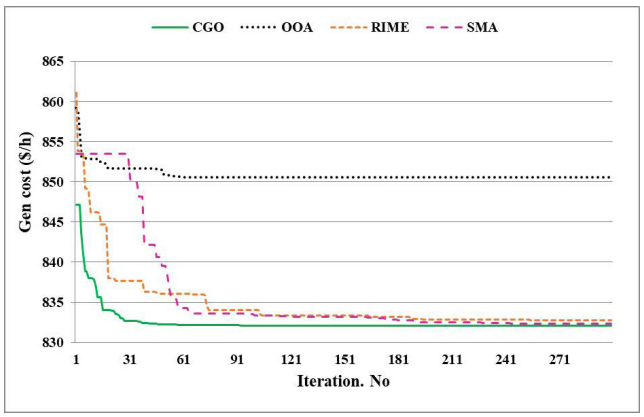

FIGURE 6. Comparison of the convergence characteristics for case 1 in IEEE 30-bus system.

1) CASE 1

In this case, the primary objective is to minimize generation costs while considering both equality and inequality

TABLE 6. Results of the suggested optimization algorithms in case 2 for the ieee 30-bus system.

Control Variable	Minimum	Maximum	CGO	OOA	RIME	SMA
$P_{Thg\,2}$(MW)	20	80	25.51022	66.593	44.4901658	25.46407
$P_{WT\,5}$(MW)	0	75	75	62.862	74.8776	75
$P_{Thg\ 8}$(MW)	10	35	34.9999	28.099	34.88299	34.99488
P_{WT11}(MW)	0	60	59.9999	44.313	53.7075	60
$P_{Thg\,13}$(MW)	12	40	39.91760	32.367	27.679	39.9280
V_1(p. u)	0.95	1.10	1.05654	1.0554	1.05445	1.0503
V_2(p. u)	0.95	1.10	1.0503472	1.055567	1.0492	1.0439
V_5(p. u)	0.95	1.10	1.039731	1.0400	1.02962	1.0324
V_8(p. u)	0.95	1.10	1.0450523	1.0472	1.03837	1.0392
V_{11}(p. u)	0.95	1.10	1.099651	1.0594	1.07087	1.09791
V_{13}(p. u)	0.95	1.10	1.07797	1.06668	1.06053	1.08515
T_{11}(p. u)	0.90	1.10	1.026840	1.064	1.0479	0.9986
T_{12}(p. u)	0.90	1.10	0.9099	1.0414	0.90987	0.94445
T_{15}(p. u)	0.90	1.10	1.009414	1.0460	1.04406	1.01318
T_{36}(p. u)	0.90	1.10	0.969993	1.02061	0.98637	0.9548
P_{Stack}	50	200	50	52.1736	50.0124	50.0622
$Q_{Thg\,1}$(MVAr)	-20	150	-0.27	-13.9	-0.86	-1.4
$Q_{Thg\,2}$(MVAr)	-20	60	13.07	17.41	18.63	10.01
Q_{WT5}(MVAr)	-30	35	23.27	21.98	16.5	21.51
$Q_{Th\,8}$(MVAr)	-15	48.7	41.88	36.94	40.86	38.46
$Q_{WT\ 11}$(MVAr)	-25	30	29.5	29.96	26.42	28.72
$Q_{Thg\,13}$(MVAr)	-15	44.7	22.52	36.45	28.97	32.03
C_{gen}($/h)			940.0360	912.8216	916.2173	940.1094
P_{loss}(Mw)			2.0277913	3.0083379	2.250450	2.049152
C_{gross}($/h)			1142.8	1213.7	1141.3	1145
VD(p. u.)			0.3715	0.6289	0.3715	0.6283
Emission			0.1415	0.1435	0.1410	0.1416

constraints. The simulation results in Table 5 compare the performance of CGO with other techniques (OOA, RIME, and SMA). Upon incorporating the wind turbines (WT) as anticipated, the total objective function of CGO decreases from 832.0665 $/h to 807.88474 $/h. This reduction in the overall objective function is attributed to the decrease in load demand achieved by integrating the WT, resulting in lower fuel costs for conventional generators. The generation costs for other algorithms are 809.005 $/h for RIME, 813.9549 $/h for OOA, and 807.9107 $/h for SMA. These results indicate that the proposed CGO outperforms alternative approaches in addressing the OPF problem with the inclusion of wind turbines. This is further illustrated in Figure 6, which demonstrates the strategy with the lowest cost and fewest iterations required by CGO compared to other algorithms. Additionally, all techniques exhibit a decrease in power losses across transmission lines, with values of 5.7 MW for CGO, 6.0809 MW for RIME, 6.2967 MW for OOA, and 5.8254 MW for SMA. Moreover, as shown in the table, the integration of wind turbines has a positive effect on reducing emissions and improving voltage across all buses.

2) CASE 2

In this section, the impact of wind turbine placement on transmission losses is evaluated, with the primary objective being to minimize active power losses to the lowest possible level, as shown in Table 6. The results indicate that the CGO algorithm outperforms other techniques in terms of achieving lower active power losses. Specifically, the CGO algorithm achieves a minimum active power loss of 2.0277913 MW, which is lower than the values obtained with RIME (2.250450 MW), OOA (3.0083379 MW), and SMA (2.049152 MW). However, it should be noted that the generation cost in this case is higher compared to the values obtained in Case 1. To assess the convergence rate of the proposed technique, the number of iterations required for achieving the best power loss is calculated. A comparison for the IEEE-30 system is presented in Figure 7, demonstrating that the CGO algorithm achieves the best results with a lower number of iterations.

3) CASE 3

By analyzing Cases 1 and 2, it becomes evident that Case 1 exhibits a larger loss, whereas Case 2 incurs considerably higher production costs. This observation emphasizes the necessity of a target that encompasses both cost and loss considerations. Introducing a cost model that converts the loss into an equivalent energy cost proves to be a straightforward approach for addressing both objectives, as indicated in Table 7. Figure 8 provides a graphical representation of the conversion curve, illustrating the gross cost comparison between CGO and other techniques. Table 7 further demonstrates that the gross cost for CGO is $1128.4142 per hour, which is lower than the values for RIME ($1128.5 per

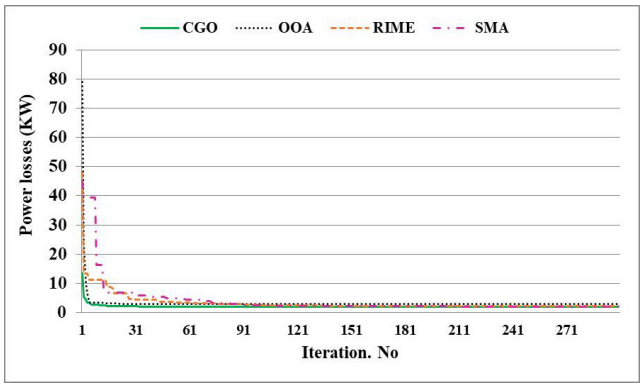

FIGURE 7. Comparison of convergence characteristics for case 2 in IEEE 30-bus system.

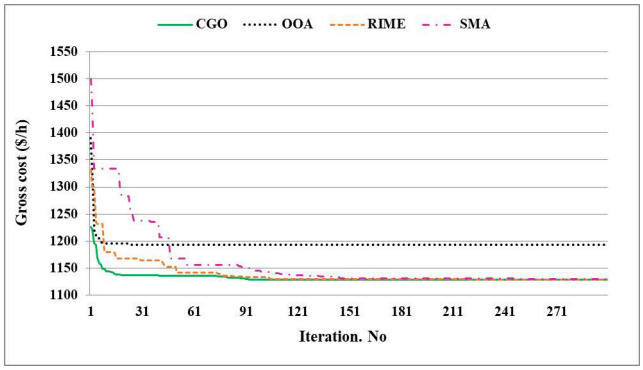

FIGURE 8. Comparison of convergence characteristics for case 3 in IEEE 30-bus system.

hour), OOA ($1187.9800 per hour), and SMA ($1130.169 per hour). Moreover, there is a significant reduction in power loss and generation cost, albeit less pronounced compared to Cases 1 and 2.

C. WIND AND PV

The IEEE 30-bus test network was modified to incorporate two renewable energy sources, specifically a wind farm (WT) and solar PV generation. Within the electrical network, there are two wind turbines and one PV unit. The first wind turbine is connected to bus 5, with a power rating of 75 MW and 25 turbines. Its nominal wind speed is 7.976 m/s. The second wind turbine farm is linked to bus 11, with a power rating of 60 MW and 20 turbines, and its nominal wind speed is 8.862 m/s. Additionally, a solar PV generator is connected to bus 13, with a rated power of 50 MW. The solar irradiance, which determines the electrical output of the PV generator, is measured at 483 W/m 2.

1) CASE 4

The outcomes of the OPF analysis, considering the projected wind turbine and solar PV generation, are presented in Table 3. Notably, in case 4, the total fuel cost exhibited a significant reduction compared to the base case and case 1 (OPF with WT). For instance, the generation cost in the base case, utilizing the proposed CGO algorithm, was determined to be $832.0665 per hour, while in case 1 it was $807.88474 per hour. However, in case 4, it decreased to $775.8345 per hour, reflecting a reduction of 7.24% compared to the base case. Furthermore, the generation cost for all other algorithms also decreased compared to the base case and case 1. As the generation cost reached its minimum value in case 4, there was a corresponding decrease in power loss across the transmission line.

Table 8 provides a detailed analysis of the outcomes achieved through the proposed CGO algorithm, aligning with the desired objectives. The total costs for CGO, OOA, RIME, and SMA were determined to be $775.8345 per hour, $788.119 per hour, $800.2959 per hour, and $776.443 per hour, respectively. These values were found to be lower than the results obtained from other algorithms, as presented in Table 8, such as $782.2 for ABC [18], $785.71 for GOA [19], $782 for GWO [20], and $782.01 for SHADE-SF [19]. Additionally, Figure 9 showcases the convergence properties of the CGO algorithm in comparison to other algorithms.

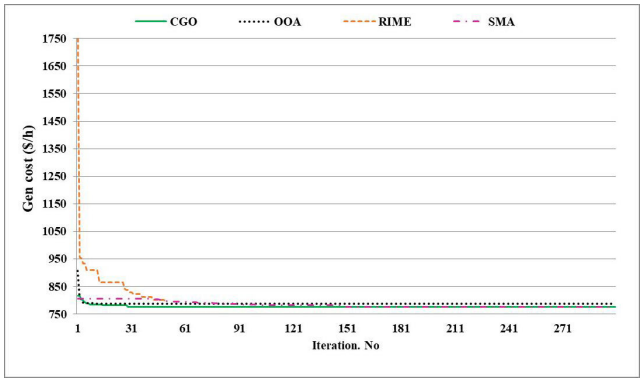

FIGURE 9. The convergence curve of an objective function (Case 4) for a 30-bus system using the CGO and other algorithms.

2) CASE 5

Optimum control variables and objective function values for CGO with other techniques for case 5 are presented in Table 9. Based on these results, it is evident that the CGO approach yields the minimum values for active power loss. Specifically, the CGO algorithm achieves a power loss result of 2.0056 MW, outperforming other algorithms such as RIME (3.4112 MW), OOA (2.1814 MW), and SMA (2.0199 MW). Thus, CGO demonstrates the most favorable outcome in this regard. Comparatively, the power loss obtained in this case is similar to that of case 2, with only a marginal difference. Furthermore, the increase in renewable energy sources has a substantial impact on reducing emissions. The emissions in CGO amount to 0.0942 t/h, while RIME records 0.0931 t/h, OOA shows 0.0990 t/h, and SMA indicates 0.0991 t/h. These values are lower than those in scenario 2 by 0.50% in CGO, 0.51% in RIME, 0.45% in OOA, and 0.43% in SMA. Despite achieving the lowest possible power loss in case 5, the overall

TABLE 7. Optimal results for different algorithms on case 3.

Control Variable	Minimum	Maximum	CGO	OOA	RIME	SMA
$P_{Thg\,2}$(MW)	20	80	41.394893	54.66977	41.2220	41.376349
$P_{WT\,5}$(MW)	0	75	74.99997	61.466	75	75
$P_{Thg\,8}$(MW)	10	35	34.999994	30.109	34.94305	34.9994
P_{WT11}(MW)	0	60	59.9999	52.75675	60	59.999
$P_{Thg\,13}$(MW)	12	40	24.12706	35.998	24.533188	24.13079
V_1(p.u)	0.95	1.10	1.0595050	1.0608	1.06214	1.0597
V_2(p.u)	0.95	1.10	1.054406716	1.05871	1.0555	1.05438
V_5(p.u)	0.95	1.10	1.043252	1.03695	1.044158	1.04273
V_8(p.u)	0.95	1.10	1.047335	1.0520	1.0482	1.04614
V_{11}(p.u)	0.95	1.10	1.0970334	1.0519	1.1	1.0947
V_{13}(p.u)	0.95	1.10	1.0835886	1.0424	1.0704	1.0886
T_{11}(p.u)	0.90	1.10	1.01157	1.05191	1.02976	1.01099
T_{12}(p.u)	0.90	1.10	0.909	1.0546	0.916517	0.902519
T_{15}(p.u)	0.90	1.10	1.013722	1.0655	1.0098	1.0292
T_{36}(p.u)	0.90	1.10	0.989516	1.02999	0.96252	0.95170
P_{Slack}	50	200	50	51.1222	49.8173	50.0004
$Q_{Thg\,1}$(MVAr)	-20	150	-2.23	-8.57	2.41	-0.77
$Q_{Thg\,2}$(MVAr)	-20	60	11.7	21.19	11.18	12.28
$Q_{WT\,5}$(MVAr)	-30	35	23.19	16.92	23.25	23.39
$Q_{Thg\,8}$(MVAr)	-15	48.7	40.39	46.24	42.27	40.93
$Q_{WT\,11}$(MVAr)	-25	30	28.07	23.28	29.94	28.31
$Q_{Thg\,13}$(MVAr)	-15	44.7	28.98	30.00	19.85	23.83
C_{gen}($/h)			916.2211	918.0005	916.9617	914.4714
P_{loss}(Mw)			2.1219	2.7224	2.1156	2.1568
C_{gross}($/h)			1128.4142	1193.491	1128.5	1130.169
VD(p.u.)			0.7150	0.7226	0.7486	0.5657
Emission			0.1422 0.1422	0.1400	0.1421	0.5657

fuel cost is higher than that in case 4. When considering all strategies, the recommended CGO algorithm consistently delivers superior results and arrives at the optimal solution with fewer iterations, as depicted in Figure 10.

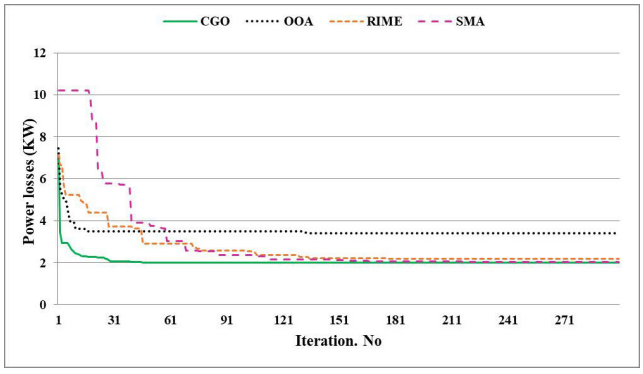

FIGURE 10. The convergence curve of an objective function (Case 5) for a 30-bus system using the CGO and other algorithms.

3) CASE 6

In cases 4-6, the minimum gross cost is achieved by minimizing the generation cost. Specifically, the gross cost values obtained are (as shown in Table 10) as follows: $1079.967 per hour for CGO, $1083.9434 per hour for RIME, $1131.85 per hour for OOA, and $1080.1504 per hour for SMA. These values are lower than those in case 3 by 0.044% for CGO, 0.41% for RIME, 0.054% for OOA, and 0.046% for SMA. This indicates that CGO performs the best among the considered algorithms, yielding the most favorable outcomes. Additionally, in case 6, the lowest gross cost is achieved compared to previous cases.

The inclusion of three renewable energy sources in place of thermal units in the electrical network contributes to the significant reduction in emissions in this case.

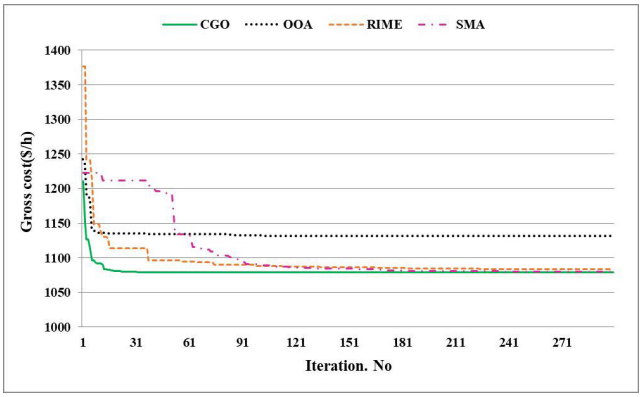

FIGURE 11. The convergence curve of an objective function (Case 6) for a 30-bus system using the CGO and other algorithms.

Figure 11 illustrates the comparison of the gross cost conversion curve for case 6 across various strategies,

TABLE 8. Optimal results for CGO compared with different algorithms on case 4.

			CGO	OOA	RIME	SMA	ABC [18]	GOA [19]	BWOA [19]	GSA [19]	SHADE-SF [19]	GWO [20]	PSO [20]
PTh2	20	80	30.600	33.2400	46.2807	27.5134	26.94	28.066	29.85	30.9	29.106	28.3	28.04
PWT_5	0	75	41.7433	42.285	34.2694	42.6871	10.01	42.766	43.68	43.4	44.084	43.82	43.74
PTh8	10	35	10.0920	16.616	15.705	10	43.19	12.241	13.94	10	10	10	10
PWT_11	0	60	35.5530	29.228	28.1665	37.7868	35.75	36.468	33.24	34.7	37.226	36.57	37.19
PPV	0	50	36.6626	33.093	30.643	34.3398	38.38	35.505	33.58	35.3	33.839	35.41	35.3
V1	0.95	1.10	1.08560	1.0754	1.08656	1.0529	1.072	1.0241	1.075	1.08	1.0724	1.1	1.082
V2	0.95	1.10	1.06811	1.0605	1.04386	1.0471	1.056	1.0973	1.057	0.96	1.0575	0.95	0.95
V5	0.95	1.10	1.03633	1.0357	0.98007	1.0300	1.035	1.0019	1.037	1.05	1.0356	1.1	1.1
V8	0.95	1.10	1.03407	1.0285	0.99763	1.02503	1.039	1.0747	1.044	1.05	1.0398	1.1	1.1
V11	0.95	1.10	1.04648	1.06484	1.0517	1.08145	1.095	1.0606	1.075	1.09	1.0998	1.1	1.1
V13	0.95	1.10	0.9807	1.036	1.01816	1.0289	1.048	1.0642	1.045	1.1	1.0543	1.1	1.063
T11	0.90	1.10	1.06425	1.01885	0.9296	0.957469	-	-	-	-	-	-	-
T12	0.90	1.10	0.95274	1.0225	0.9169	1.02083	-	-	-	-	-	-	-
T15	0.90	1.10	0.9825	1.0065	0.95107	0.9913	-	-	-	-	-	-	-
T36	0.90	1.10	0.97629	1.0091	0.92881	0.98097	-	-	-	-	-	-	-
PSlack	50	140	134.918	134.970	136.185	137.221	134.9	134.91	134.9	135	134.91	134.9	134.9
QTh1	-20	150	13.23	2.54	74.90	-21.28	-1.23	-20	5.307	17.3	-1.9239	146.8	15.68
QTh2	-20	60	32.86	24.84	8.64	35.26	13.01	60	7.631	-20	13.266	-18.4	-20
QW5	-30	35	22.01	26.26	0.69	31.98	36.65	-5.6282	25.47	31.6	23.278	-15	35
QTh8	-15	40	35.03	21.87	37.15	38.94	23.79	40	40	37.9	35.11	35	40
QW11	-25	30	25.75	25.65	4.02	22.36	29.64	19.217	22.35	24.5	30	3.584	27.86
QPV13	-20	25	-7.67	15.90	-0.23	12.15	15.24	25	15.37	25	17.249	25	17.73
Cost			775.834	788.119	800.295	776.443	782.2	785.71	784.81	782.2	782.01	782	781.9
Loss			6.1701	6.0039	7.8510	6.1490	-	-	-	-	-	-	-
Gross cost			1400	1392	1586.5	1399	-	-	-	-	-	-	-
VD			0.6224	0.5198	0.2936	0.3711	-	-	-	-	-	-	-
Emission			0.1596	0.1578	0.1585	0.1638	-	-	-	-	-	-	-

highlighting CGO as the approach with the lowest cost and requiring fewer iterations compared to other strategies. When considering all techniques, the suggested CGO algorithm consistently produces superior results and converges to the global best solution with fewer iterations.

D. WIND AND FACTS DEVICES

In this section, we will examine how the integration of renewable energy sources in specific locations affects the performance of OPF solvers and the IEEE 30-bus system, which includes FACTS devices. The presence of FACTS devices enables the maximization of the transmission line's thermal limit, thereby minimizing system congestion. This reduction in congestion leads to a decrease in the cost of system generation and also lowers the overall system risk. Increasing the number of wind farms offers the most cost-effective system generation option, resulting in enhanced societal benefits. The results indicate that the inclusion of FACTS devices in the network improves the voltage profile, reduces power losses, lowers generation costs, and enhances the stability of the power network's operation. Furthermore, the application of metaheuristic optimization reveals that the introduction of FACTS devices has a significant impact on OPF solutions whenever the network expands to incorporate them.

1) CASE 7

Based on the data provided in Table 11, it is evident that the placement of FACTS devices in optimal locations with suitable ratings resulted in a reduction in the total generation cost. Specifically, in the CGO algorithm, the total generation cost decreased to \$807.0393/h, which is lower than the costs observed in the RIME algorithm (\$808.5072/h), OOA algorithm (\$817.0351/h), and SMA algorithm (\$807.496018/h). Additionally, the CGO algorithm's cost was lower compared to other algorithms studied, such as MVO [21] (\$808.030/h), ALO [21] (\$809.449/h), SCA [21] (\$818.654/h), CBA [22] (\$810.5056/h), FPA [22] (\$808.0864/h), and SCA [22] (\$815.4325/h), as shown in Figure 12. This indicates that the CGO approach yielded a lower cost compared to the other algorithms. Furthermore, in the CGO algorithm, the real power loss was measured at 5.5071 MW, which is

TABLE 9. Optimum control variables and objective function values for CGO with other techniques for case 5.

			CGO	OOA	RIME	SMA	GOA [19]	BWOA [19]	GWO [19]	SHADE-SF [19]	ALO [19]	GSA [19]	PSO [19]
PTh2	20	80	24.8666	67.5610	31.59221	22.13554	20.529	28.192	50.833	40.8878	28	49.2	25.4
PWT_5	0	75	74.9999	59.742	75	75	75	68.112	56.529	73.3288	75	63.3	75
PTh8	10	35	34.9997	29.4185	35	34.1376	34.181	49.413*	14.759	31.638	33.7	35	35
PWT_11	0	60	59.999	41.817986	60	59.9652	60	59.042	60	56.6613	60	54.3	60
PPV	0	50	40.5392	20.1776	30.1126	44.18168	49.999	30.782	46.613	36.6769	38.8	31.6	40
V1	0.95	1.10	1.05871	1.063477	1.0636	1.05441	0.9918	1.0611	0.95	0.9897	1.06	1.04	1.06
V2	0.95	1.10	1.0526	1.05293	1.05652	1.048758	1.0554	1.0548	1.0007	1.056	1.05	1.07	1.1
V5	0.95	1.10	1.042130	1.04741	1.0419	1.039323	1.0708	1.0417	1.0725	1.0956	1.05	1.04	1.1
V8	0.95	1.10	1.047456	1.0393	1.0431	1.04362	1.0917	1.0525	1.0537	1.0422	1.09	1.07	1.1
V11	0.95	1.10	1.095562	1.05683	1.09161	1.1	1.0859	1.0898	1.0221	1.0981	1.1	1.09	1.06
V13	0.95	1.10	1.075880	1.03463	1.0488	1.0764	1.0819	1.0463	1.1	1.0805	1.05	1.04	5.46
T11	0.90	1.10	1.01521	1.02877	0.96187	1.029469	-	-	-	-	-	-	-
T12	0.90	1.10	0.9006	1.0391	1.087310	0.9	-	-	-	-	-	-	-
T15	0.90	1.10	0.99759	1.04607	1.0110	0.99796	-	-	-	-	-	-	-
T36	0.90	1.10	0.96099	1.0099	0.98717	0.957226	-	-	-	-	-	-	-
PSlack	50	140	50	68.0932	53.8767	49.9997	50	50	63.381	50.8831	50	53.2	50
QTh1	-20	150	-3.65	4.93	0.54	-5.24	-20	-2.096	-20	-20	-4.97	-20	5.46
QTh2	-20	60	7.62	-7.46	12.76	7.75	6.2084	9.084	-20	16.8815	6.79	36.6	-20
QW5	-30	35	20.7	33.31	19.50	21.46	35	19.824	35	35	20.9	14.9	35
QTh8	-15	40	38.44	31.70	32.33	36.33	40	39.939	40	22.3922	40	40	40
QW11	-25	30	27.26	24.13	25.21	29.76	23.497	27.895	0.6872	29.7924	30	26.7	30
PV13	-20	25	20.91	24	20.52	21.98	25	14.144	25	25	16.5	10.5	19
Loss	-	-	2.0056	3.4112	2.1814	2.01991	2.2043	2.1403	2.0616	2.3235	2.08	2.55	2.16
COST	-	-	880.4118	873.1812	880.2888	881.9733	-	-	-	-	-	-	-
Gross cost	-	-	10881	1214	1099	1084	-	-	-	-	-	-	-
VD	-	-	0.8046	0.6144	0.4132	0.7626	-	-	-	-	-	-	-
Emission	-	-	0.0942	0.0990	0.0931	0.0951	-	-	-	-	-	-	-

** Infeasible solution*

TABLE 10. Optimal results for the suggested methods on case 6.

			CGO	OOA	RIME	SMA
	Min	Max				
PTh2	20	80	27.9620	51.78034	25.7367	28.322134
PWT_5	0	75	74.9968	63.7957	74.97326	74.9998848
PTh8	10	35	34.6256	32.6315	34.9220	34.8096
PWT_11	0	60	59.9722	54.3279	59.949	58.8502
PPV13	0	50	37.86939	43.6939	40.74848	38.6105
V1	0.95	1.10	1.05583	1.0557	1.055594	1.05794
V2	0.95	1.10	1.050581	1.04737	1.048577	1.051724
V5	0.95	1.10	1.043657	1.04579	1.0418	1.043307
V8	0.95	1.10	1.047376	1.04191	1.04165	1.04890
V11	0.95	1.10	1.095426	1.087452	1.09717	1.1
V13	0.95	1.10	1.07635	1.0645	1.07085	1.073237
T11	0.90	1.10	1.020181	1.00871	1.01422	1.0136927
T12	0.90	1.10	0.907764	1.0593	0.92468	0.91239
T15	0.90	1.10	0.99999	1.05731	1.024025	1.0069
T36	0.90	1.10	0.9665	1.006617	0.96382	0.955948
PSlack	50	140	49.9916	39.5880	49.0970	49.8294
QTh1	-20	150	-6.04	1.93	-2.25	-3.84
QTh2	-20	60	5.04	-15.05	2.14	0.0334
QW5	-30	35	23.63	31.39	24.31	0.2169
QTh8	-15	40	39.94	25.84	31.34	39.18
QW11	-25	30	27.31	29	30	0.2960
QPV13	-20	25	21.37	23	24.26	20.36
Cost	-	-	879.4959	887.0677	882.2639	879.1316
Loss	-	-	2.0178	2.4175	2.0270	2.0218
Gross cost	-	-	1079.967	1131.85	1083.9434	1080.150494
VD	-	-	0.7981	0.4889	0.6212	0.7719
Emission	-	-	0.0934	0.0909	0.0939	0.0933

TABLE 11. Optimal simulation results for CGO compared with different algorithms on case 7.

Control Variable	Minimum	Maximum	CGO	OOA	RIME	SMA	MVO [21]	ALO [21]	SCA [21]	CBA [22]	FPA [22]	SCA [22]
$P_{Thg\,2}$(MW)	20	80	39.5027	45.057	37.67556	40.06264	40.311	40.960	35.458	34.2203	42.0349	36.9766
$P_{WT\,5}$(MW)	0	75	49.6066	38.088	50.8397	49.617535	49.459	49.077	41.719	46.3742	48.6959	54.1868
$P_{Thg\ 8}$(MW)	10	35	10.0052	17.863	10	10.00001	10.352	13.038	15.172	11.4817	10.2470	10
P_{WT11}(MW)	0	60	42.88457	37.901	43.7626	42.4557	42.135	39.362	47.561	46.9442	40.4740	42.6132
$P_{Thg\,13}$(MW)	0	50	12	15.858	12	12	12.000	12.000	14.321	13.2978	12.5667	12
V_1(p.u)	0.95	1.10	1.07452	1.0654	1.06689	1.06841	1.100	1.100	1.019	1.1	1.0854	0.95
V_2(p.u)	0.95	1.10	1.0596	1.0575	1.05152	1.0533	1.090	1.091	0.992	1.09141	1.0721	0.9546
V_5(p.u)	0.95	1.10	1.03775	1.0222	1.0202	1.03076	1.071	1.072	0.978	1.07156	1.0464	0.95
V_8(p.u)	0.95	1.10	1.03761	1.0388	1.0306	1.03178	1.076	1.079	0.950	1.07709	1.0410	0.95
V_{11}(p.u)	0.95	1.10	1.09271	1.04297	1.0662	1.09482	1.100	1.071	1.047	1.1	1.0563	1.1
V_{13}(p.u)	0.95	1.10	1.07271	1.0850	1.07557	1.0711	1.062	1.038	0.950	1.1	1.0325	1.1
T_{11}(p.u)	0.90	1.10	1.028357	1.0023	0.96128	1.0107	1.007	1.059	0.959	1.02354	1.0388	0.9
T_{12}(p.u)	0.90	1.10	0.917681	1.0093	0.987981	0.90036	1.087	1.084	0.900	0.90941	0.9448	1.1
T_{15}(p.u)	0.90	1.10	0.990180	1.0238	1.07562	1.0054	1.099	1.095	0.938	1.06355	1.0590	0.9
T_{36}(p.u)	0.90	1.10	0.966798	1.0030	0.94288	0.969629	1.024	1.087	0.900	0.94385	0.9816	0.9
τ_{TCSC1}(%)	0	50%	0.262668	0.4525	26	0	0.219	0.218	0	28.8775	16.5410	5.5742
τ_{TCSC2}(%)	0	50%	0.26757811	0.2637	24	0.15763	0.239	0.440	0	9.7268	23.9199	28.5700
$\emptyset_{TCSC1}$(deg)	-5	5	3.673519	-1.45420	1	2.08499	4.503	-3.99	3.917	0.1637	1.1265	2.3692
$\emptyset_{TCSC2}$(deg)	-5	5	2.5974158	-0.1190	14	-1.0197	3.761	-4.281	1.150	-1.257	1.1640	-0.0104
Q_{SVC1}(MVAr)	-10	10	5.45977	6.9852	15	9.7537	9.893	-6.541	3.882	-9.3060	-2.318	8.5249
Q_{SVC2}(MVAr)	-10	10	8.671660	-1.6127	14	1.21561	-6.277	1.209	5.482	-3.2700	8.2846	3.6386
TCSC1 Branch	1	40	2	31	0.266910	1	39	10	3	-	-	-
TCSC2 Branch	1	41	5	19	0.2365	36	29	20	4	-	-	-
TCPS1 Branch	1	40	11	8	-0.13700	35	16	34	15	-	-	-
TCPS2 Branch	1	41	12	23	2.90149	4	22	19	1	-	-	-
SVC1 Bus	3	29	19	25	6.13857	24	27	6	19	-	-	-
SVC2 Bus	3	30	24	12	1.3330	8	27	10	9	-	-	-
P_{Slack}	50	200	134.908	134.89	134.9134	134.9182	-	-	-	-	-	-
$Q_{Thg\,1}$(MVAr)	20 -	150	2.75	-13.93	0.97	3.06	-	-	-	-	-	-
$Q_{Thg\,2}$(MVAr)	20 -	60	17.81	39.2	21.23	17.66	-	-	-	-	-	-
$Q_{Thg\,8}$(MVAr)	30	35	24.35	15.81	16.31	24.76	-	-	-	-	-	-
Q_{WT5}(MVAr)	15	48.7	34	43.35	43.72	35.84	-	-	-	-	-	-
Q_{W11}(MVAr)	-25	30	24.11	10.44	12.44	25.79	-	-	-	-	-	-
$Q_{PV\,13}$(MVAr)	-15	44	17.5	37.92	38.37	20.01	-	-	-	-	-	-
C_{gen}($/h)	-	-	807.0393	817.0351	808.5072	807.496018	808.030	809.449	818.654	810.5056	808.0864	815.4325
P_{loss}(Mw)	-	-	5.5071	6.2547	5.7913	5.6542	-	-	-	-	-	-
C_{gross}($/h)	-	-	1357.7	1442.5	1387.6	1372.9	-	-	-	-	-	-
VD(p.u.)	-	-	0.9031	0.3847	0.4761	0.7959	-	-	-	-	-	-
Emission	-	-	0.2136	0.2101	0.2139	0.2136	-	-	-	-	-	-

lower than 6.1701 MW in Case 1 and 5.7769 MW in Case 4. This reduction in power loss directly impacted the gross cost, where the CGO algorithm resulted in $1357.7/h, which is lower than the costs observed in the RIME algorithm ($1387.6/h), OOA algorithm ($1442.5/h), and SMA algorithm ($1372.9/h).

2) CASE 8

In this particular scenario, the influence of FACTS devices on decreasing power losses within the electrical transmission network is evidently more significant than in other instances. The power loss attained by CGO amounts to 1.761859 MW, which is lower than the values of 2.2278212 MW in RIME, 2.8777 MW in OOA, 1.9416 MW in SMA, 2.482 MW in SCA [21], 1.880 MW in IMO [21], 1.7898 MW in GWO [22], 1.9736 MW in FPA [22], and 2.0420 MW in SCA [22]. As illustrated in Table 12, all algorithms exhibit reduced power losses compared to previous cases. Furthermore, Figure 13 displays the convergence curve of CGO in comparison to other algorithms, demonstrating its ability to reach the optimal value in a fewer number of iterations.

3) CASE 9

Optimal simulation results for CGO compared with different algorithms on Case 9 are tabulated in Table 13. In Case 9, the CGO method achieved an optimal gross cost value of 1105.6378 $/h, which is lower than the minimal goal values of other methods, namely 1121.5043 $/h in RIME, 1184.2 $/h in OOA, and 1105.996 $/h in SMA. Furthermore,

TABLE 12. Optimal simulation results for CGO compared with different algorithms on case 8.

Control Variable	Minimum	Maximum	CGO	OOA	RIME	SMA	SCA [21]	IMO [21]	GWO [22]	FPA [22]	SCA [22]
$P_{Thg\,2}$(MW)	20	80	25.16201	58.94823	41.1972	25.8516	80.000	79.644	25.1902	47.3912	58.5751
$P_{WT\,5}$(MW)	0	75	74.99987	64.24453	74.98450	75	73.825	74.667	75.0000	74.8351	73.9576
$P_{Thg\,8}$(MW)	10	35	34.9999	30.65109	27.1086	35	30.726	34.844	34.9999	31.4165	35.0000
P_{WT11}(MW)	0	60	59.99999	43.8374	51.53332	60	50.635	59.748	60.0000	59.3914	60.0000
$P_{Thg\,13}$(MW)	0	50	39.99996	32.4534	40	39.4885	31.706	39.832	39.9996	36.6184	40.0000
V_1(p.u)	0.95	1.10	1.05585	1.0606	1.0477	1.040215	1.098	1.089	1.0515	1.0159	1.1000
V_2(p.u)	0.95	1.10	1.050061	1.054528	1.0416	1.033859	1.091	1.089	1.0454	1.0108	1.1000
V_5(p.u)	0.95	1.10	1.04006	1.03670	1.0300	1.02547	1.100	1.089	1.0346	1.0072	1.1000
V_8(p.u)	0.95	1.10	1.0450427	1.0408	1.0348	1.02941	1.100	1.090	1.0388	1.0042	1.1000
V_{11}(p.u)	0.95	1.10	1.087141	1.0609	1.09303	1.09100	1.100	1.089	1.0865	1.0730	1.1000
V_{13}(p.u)	0.95	1.10	1.078449	1.0533	1.069348	1.08143	0.990	1.089	1.0749	1.0722	1.1000
T_{11}(p.u)	0.90	1.10	1.00826	1.0317	0.99510	1.0003	1.030	1.090	1.0243	0.9664	1.1000
T_{12}(p.u)	0.90	1.10	0.991119	1.0641	0.9519	0.9024	1.100	1.090	0.9306	0.9000	0.9000
T_{15}(p.u)	0.90	1.10	1.01121	1.051	0.98373	1.0064	1.018	1.090	1.0176	1.0294	1.1000
T_{36}(p.u)	0.90	1.10	0.984298	1.0219	0.98654	0.93425	1.100	1.090	0.9510	0.9717	1.1000
τ_{TCSC1}(%)	0	50%	0.499417	0.29998	0.19666	0.1369	0	0.471	23.7709	26.0579	3.1102
τ_{TCSC2}(%)	0	50%	0.346244	0.362210	0.0982	0.48399	0	0.498	15.4458	23.3010	28.0676
$\emptyset_{TCSC1}$(deg)	-5	5	4.183060	-0.31684	-0.32791	0.3680	4	4.979	0.0691	1.5612	5.0000
$\emptyset_{TCSC2}$(deg)	-5	5	0.318987	1.8132	-0.63848	1.5770	1	0.946	3.8477	2.0152	5.0000
Q_{SVC1}(MVAr)	-10	10	9.99985	8.2260	9.48615	5.6549	6.535	9.956	8.2708	2.8023	10-
Q_{SVC2}(MVAr)	-10	10	9.57207	3.8291	8.870182	8.1797	-0.936	4.219	6.5187	10.0000	10.0000
TCSC1 Branch	1	40	14	35	14	25	3	40	-	-	-
TCSC2 Branch	1	41	25	29	15	7	2	41	-	-	-
TCPS1 Branch	1	40	35	33	8	3	0.433	33	-	-	-
TCPS2 Branch	1	41	19	31	32	13	1.249	34	-	-	-
SVC1 Bus	3	29	21	26	22	24	11	27	-	-	-
SVC2 Bus	3	30	24	19	7	7	16	30	-	-	-
P_{Slack}	50	200	50	56.1429	50.8041	50.0013	-	-	-	-	-
$Q_{Thg\,1}$(MVAr)	20 -	150	-3.41	-0.99	-0.13	-1.11	-	-	-	-	-
$Q_{Thg\,2}$(MVAr)	20 -	60	8.35	10.16	9.14	8.5	-	-	-		-
$Q_{Thg\,8}$(MVAr)	-30	35	21.71	20.2	17.51	20.68	-	-	-	-	-
$Q_{WT\,5}$(MVAr)	15	48.7	29.81	25.47	35.78	36.03	-	-	-	-	-
$Q_{WT\,11}$(MVAr)	-25	30	22.7	28.04	25.65	24.88	-	-	-	-	-
$Q_{PV\,13}$(MVAr)	-15	44.7	25.58	32.98	17.98	25.97	-	-	-	-	-
C_{gen}($/h)	-	-	939.3405	909.9124	928.2806	938.9086	-	--	-	-	-
P_{loss}(Mw)	-	-	1.761859	2.8777	2.2278212	1.9416	2.482	1.880	1.7898	1.9736	2.0420
C_{gross}($/h)	-	-	1115.5	1997.7	1151.1	1133.1	-	-	-	-	-
VD(p.u.)	-	-	0.8390	0.4945	0.6407	0.7792	-	-	-	-	-
Emission	-	-	0.1416	0.1435	0.1410	0.1416	-	-	-	-	-

the values for GNDO [21], MVO [21], ALO [21], SCA [21], and IMO [21] are 1120.996 MW, 1125.97 MW, 1138.357 MW, 1187.287 MW, and 1148.359 MW, respectively.

Additionally, the proposed method resulted in an active power loss of 1.8789 MW, a total generation cost of 917.7474 $/h, and a voltage deviation of 0.9214 p.u.

This was achieved by strategically placing three types of FACTS devices (TCSC, SCPS, and SVC) in optimal locations with appropriate capacities. The chosen cost criteria for both thermal and renewable power units play a crucial role in determining the optimal prices and losses in this case. Taking both objectives into account, the CGO method consistently achieves the lowest gross cost. Figure 14 demonstrates the convergence curve comparison, highlighting the superior performance of the CGO method compared to other approaches.

E. DISCUSSION

An appropriate power management system is a crucial tool for establishing an economical and ecologically friendly power supply network. However, due to the lack of research on the utilization of metaheuristic algorithms for OPF problems, this paper introduces a novel optimization technique called Chaos Game Optimization (CGO), inspired by vitality. The CGO algorithm is compared with RIME, OOA, and SMA in various scenarios, and it outperforms them in most cases, as demonstrated by previous results.

Hence, the CGO algorithm is thoroughly examined to assess its performance in all cases. This section provides

TABLE 13. Optimal simulation results for cgo compared with different algorithms on case 9.

Control & State Variable	Min	Max	CGO	OOA	RIME	SMA	GNDO [21]	MVO [21]	ALO [21]	SCA [21]	IMO [21]
$P_{Thg\,2}$(MW)	20	80	39.04444	68.8212	48.7451	41.4728	44.894	47.802	55.203	20.000	56.164
$P_{WT\,5}$(MW)	0	75	74.999998	64.6076	75	74.99846	74.998	74.564	71.256	75.000	68.555
$P_{Thg\,8}$(MW)	10	35	34.99999	29.7659	30.417	34.9999	35.000	32.893	33.271	35.000	30.826
P_{WT11}(MW)	0	60	59.99991	51.0645	55.856	59.994	59.006	58.030	50.102	60.000	58.732
$P_{Thg\,13}$(MW)	0	50	26.234532	35.5941	26.3544	23.84301	21.583	22.222	32.274	19.540	23.229
V_1(p.u)	0.95	1.10	1.058152	1.05513	1.0623	1.0601	1.046	1.100	1.100	1.100	1.100
V_2(p.u)	0.95	1.10	1.052900	1.05377	1.0572	1.055756	1.042	1.097	1.098	1.100	1.100
V_5(p.u)	0.95	1.10	1.042193	1.04694	1.0439	1.044432	1.032	1.087	1.087	1.100	1.100
V_8(p.u)	0.95	1.10	1.045949	1.0504	1.04463	1.04718	1.035	1.092	1.091	1.100	1.098
V_{11}(p.u)	0.95	1.10	1.072823	1.04769	1.1	1.09329	1.098	1.100	1.100	1.100	1.100
V_{13}(p.u)	0.95	1.10	1.067288	1.06105	1.0544	1.067495	1.035	1.100	1.083	1.100	1.098
T_{11}(p.u)	0.90	1.10	0.9901295	1.0282	1.019	1.0263	1.077	1.054	1.007	1.100	1.084
T_{12}(p.u)	0.90	1.10	0.9640114	1.018958	0.9556	0.961602	0.901	0.903	1.089	1.100	1.084
T_{15}(p.u)	0.90	1.10	1.028904	1.0388	1.0088	0.9981	1.065	1.053	1.081	1.100	1.100
T_{36}(p.u)	0.90	1.10	0.987860	1.0231	0.950424	0.97309	0.985	1.001	1.033	1.100	1.087
τ_{TCSC1}(%)	0	50%	0.40191	0.4315	0.4977	0.38409	0.500	0.468	0.470	0.002	0.500
τ_{TCSC2}(%)	0	50%	0.124270	0.43322	0.44672	0.31257	0.013	0.490	0.355	0.000	0.147
$\emptyset_{TCSC1}$(deg)	-5	5	-0.482217	2.66091	0.999	-0.3061	3.173	0.486	4.591	2.761	1.494
$\emptyset_{TCSC2}$(deg)	-5	5	2.9314	2.5638	-0.7374	2.8411	-0.508	-1.527	-0.901	5.000	2.191
Q_{SVC1}(MVAr)	-10	10	9.9999	5.63735	7.5843	9.9811	9.999	-3.639	3.886	10.000	8.490
Q_{SVC2}(MVAr)	-10	10	9.99617	3.28982	8.8106	7.74069	3.844	-1.487	3.411	-0.065	7.591
TCSC1 Branch	1	40	16	34	16	29	14	7	39	1	18
TCSC2 Branch	1	41	25	35	10	19	4	29	34	3	31
TCPS1 Branch	1	40	8	32	31	30	16	4	35	31	30
TCPS2 Branch	1	41	33	31	37	33	19	2	25	11	33
SVC1 Bus	3	29	21	24	23	24	24	28	26	15	24
SVC2 Bus	3	30	24	23	17	21	13	14	26	3	10
P_{Slack}	50	200	50	35.8921	49.1410	50	-	-	-	-	-
$Q_{Thg\,1}$(MVAr)	20 -	150	-2.82	-7.18	-0.09	-.15	-	-	-	-	-
$Q_{Thg\,2}$(MVAr)	20 -	60	9.82	5.45	13.67	13.32	-	-	-	-	-
$Q_{Thg\,8}$(MVAr)	-30	35	22.46	29.33	21.76	22.36	-	-	-	-	-
$Q_{WT\,5}$(MVAr)	-15	48.7	34.36	43.24	31.77	32.21	-	-	-	-	-
$Q_{WT\,11}$(MVAr)	-25	30	15.11	17.38	28.77	26.09	-	-	-	-	-
$Q_{PV\,13}$(MVAr)	-15	44.7	25.35	29.79	12.32	16.91	-	-	-	-	-
C_{gen}($/h)	-	-	917.7474	948.6642	915.6100	915.1397	-	-	-	-	-
P_{loss}(Mw)	-	-	1.8789	2.3456	2.1149	1.9086	-	-	-	-	-
C_{gross}($/h)	-	-	1105.6378	1184.2	1128.1	1105.996	1120.996	1125.970	1138.357	1187.287	1148.359
VD(p.u.)	-	-	0.9214	0.4490	0.8466	0.8434	-	-	-	-	-
Emission	-	-	0.1417	0.1429	0.1416	0.1423	-	-	-	-	-

additional analysis and evidence to support the effectiveness of the proposed metaheuristic optimization techniques applied to cases 1-9 of the IEEE 30-bus system, particularly focusing on addressing stochastic OPF problems involving renewable energy sources. Initially, deterministic OPF cases for the original network configuration (without wind turbines and photovoltaics) are considered to showcase the efficacy of the proposed method discussed in previous sections. The suggested method is employed to solve conventional OPF problems with fixed loads in this scenario.

The suggested approach's performance was validated by comparing its results across various scenarios, with or without the incorporation of renewable energy into the system. The primary objective was to reduce the cost of the thermal generator. The population size for all algorithms was set at 100, and a maximum of 300 iterations was selected. Upon analyzing the provided data, it was found that the CGO method outperformed all other optimization algorithms by achieving the lowest cost function value across all cases. The integration of renewable energy sources (RES) into the electricity network led to decreased transmission losses and fuel running costs. The tables and Figures depicting the results of 9 cases revealed that the lowest generation cost was observed when integrating photovoltaics with a wind turbine (cases 4-6), while the lowest active power loss occurred when integrating FACTS with a wind turbine. The proposed CGO technique exhibited superior performance compared to other techniques (OOA, RIME, and SMA) mentioned in this paper and previous article. Objective function comparisons for all

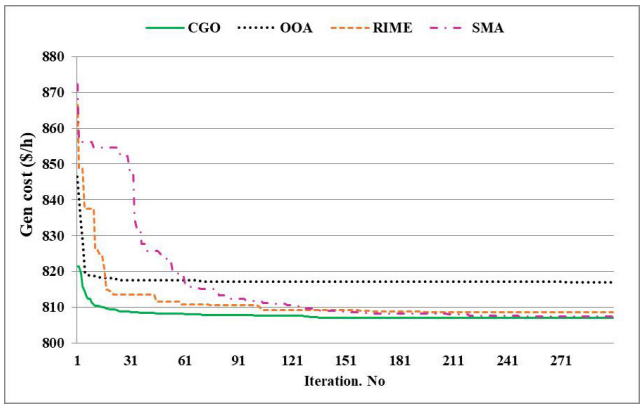

FIGURE 12. Comparison of convergence characteristics of three techniques with CGO for Case 7.

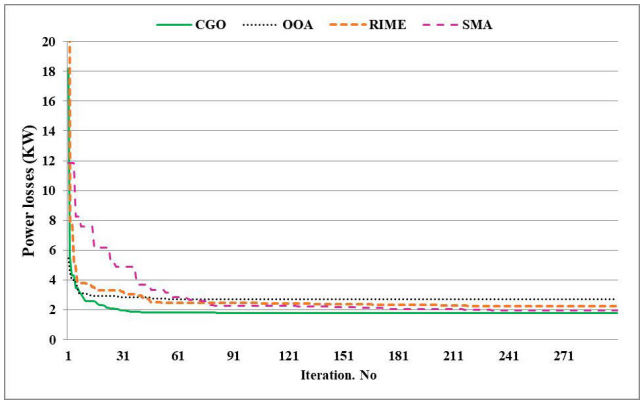

FIGURE 13. The convergence properties of CGO with other algorithms for Case 8.

cases can be observed in Figures 15-17, while Figures 18-19 illustrate the emission and voltage deviation across different scenarios. Notably, there were significant improvements in the voltage profile, and maintaining acceptable load bus voltages between 0.95 and 1.05 p.u. was crucial for the optimal power flow problem. The voltage profiles of load buses for all cases are depicted in Figures 20-22.

Figure 23 presents the optimal schedule of active power generated by the generator for cases 1-3, while

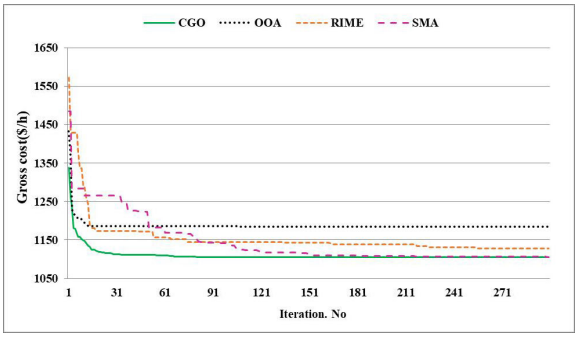

FIGURE 14. Comparison of the convergence properties of three approaches with CGO for Case 9.

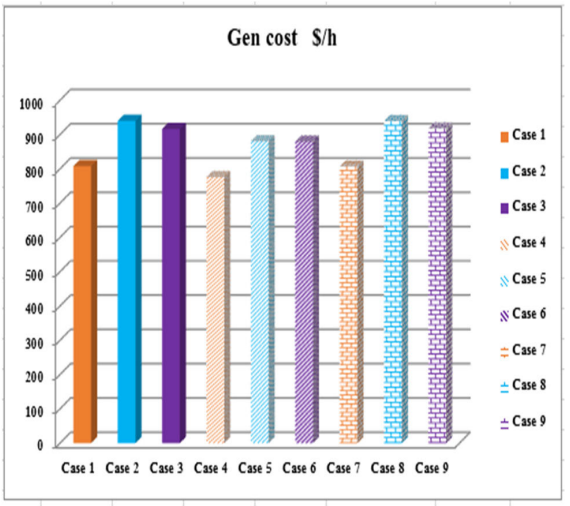

FIGURE 15. The generation cost (Objective function) obtained in the three cases for all scenarios by CGO algorithm.

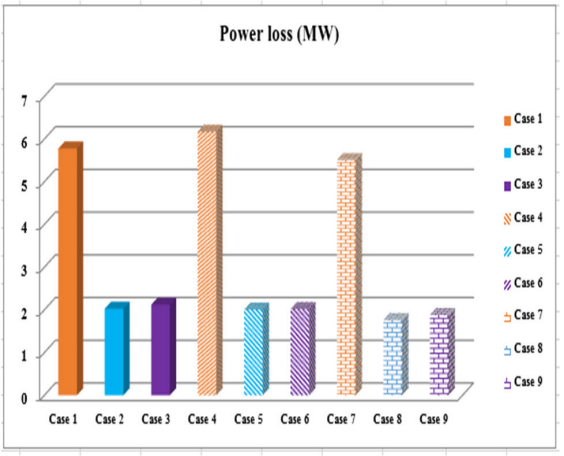

FIGURE 16. The power loss (Objective function) obtained in the three cases for all scenarios by CGO algorithm.

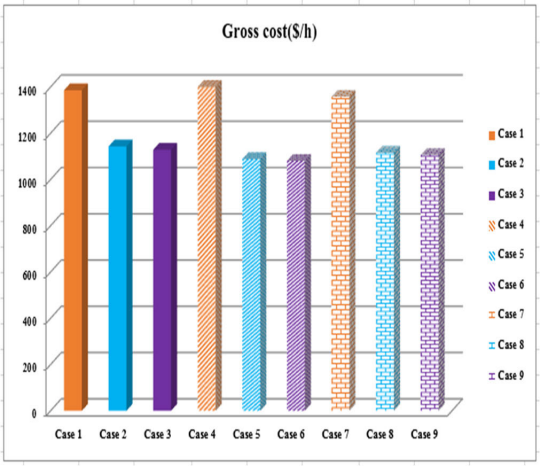

FIGURE 17. The Gross cost (Objective function) obtained in the three cases for all scenarios by CGO algorithm.

Figures 24 and 25 display the corresponding schedules for cases 4-6 and cases 7-8, respectively. In the con-

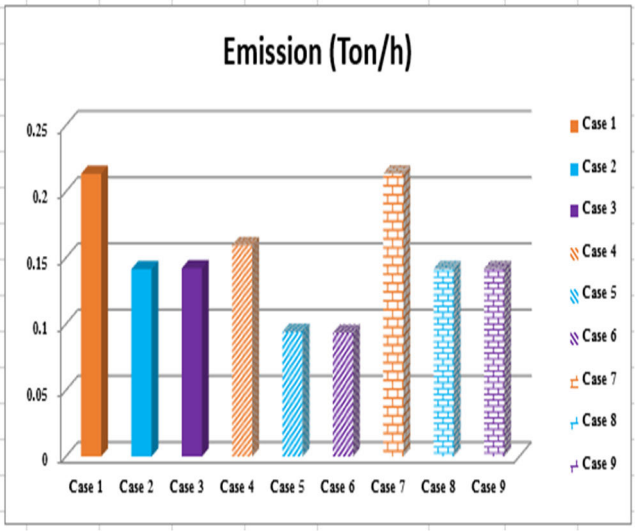

FIGURE 18. The Emission obtained in the all cases by CGO algorithm.

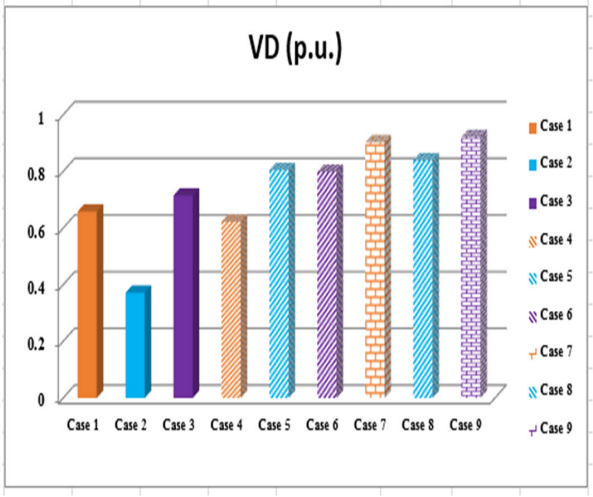

FIGURE 19. The Emission obtained in the all cases by CGO algorithm.

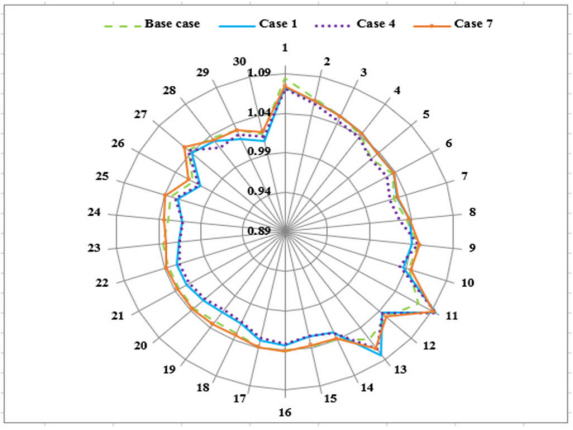

FIGURE 20. Comparison of voltage profile of busses for all scenario in gen cost in IEEE 30-bus.

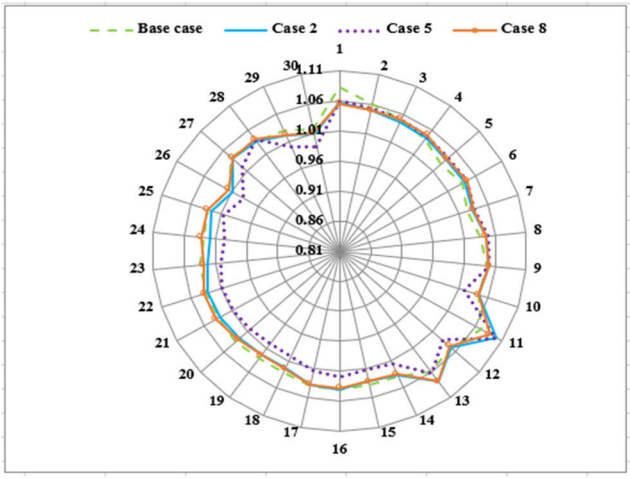

FIGURE 21. Comparison of voltage profile of buses for all scenario in ploss in IEEE 30-bus.

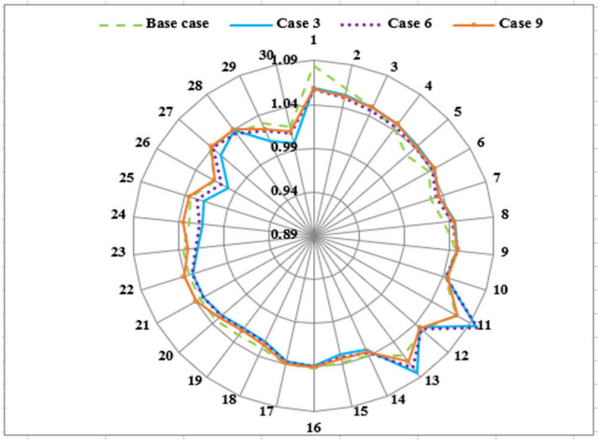

FIGURE 22. Comparison of voltage profile of buses for all scenario in gross in IEEE 30-bus.

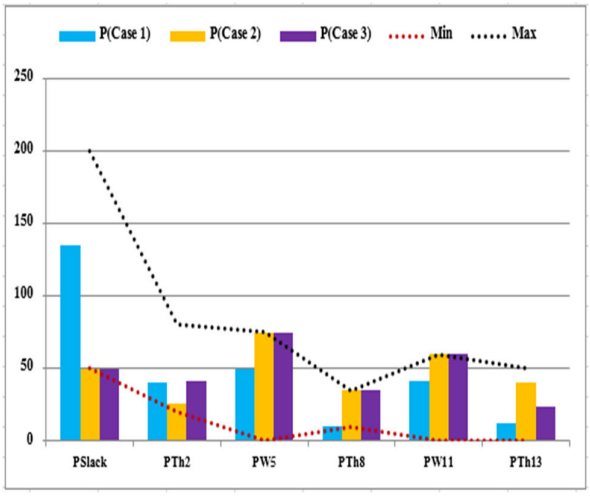

FIGURE 23. Optimal scheduled actual power (MW) for Cases 1, 2, and 3.

text of the optimal power flow problem, the dependent variable or state of interest is the generation of reactive power. It is crucial to ensure that the reactive power constraints are satisfied during the optimization process.

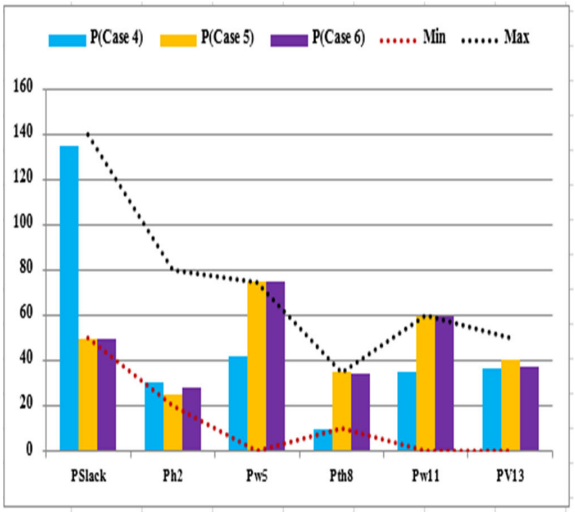

FIGURE 24. Optimal scheduled actual power (MW) for Cases 4, 5, and 6.

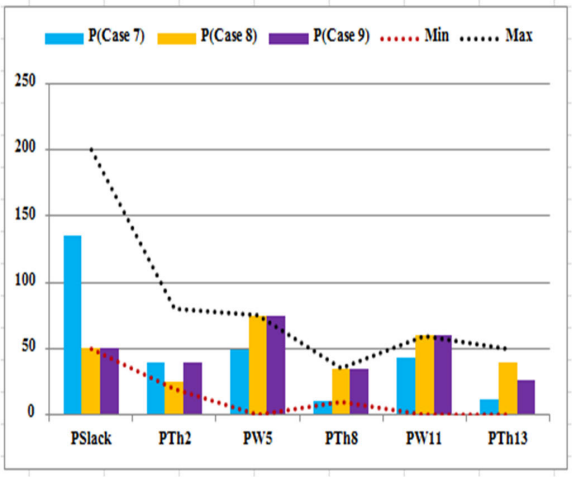

FIGURE 25. Optimal scheduled actual power (MW) for Cases 7, 8, and 9.

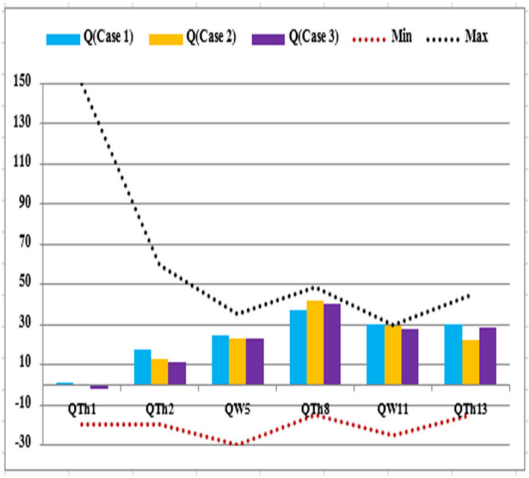

FIGURE 26. Schedule for reactive power from the generators for Cases 1, 2, and 3.

Figures 26-28 illustrate the reactive power schedules for all generators. Upon examining the constraints outlined in

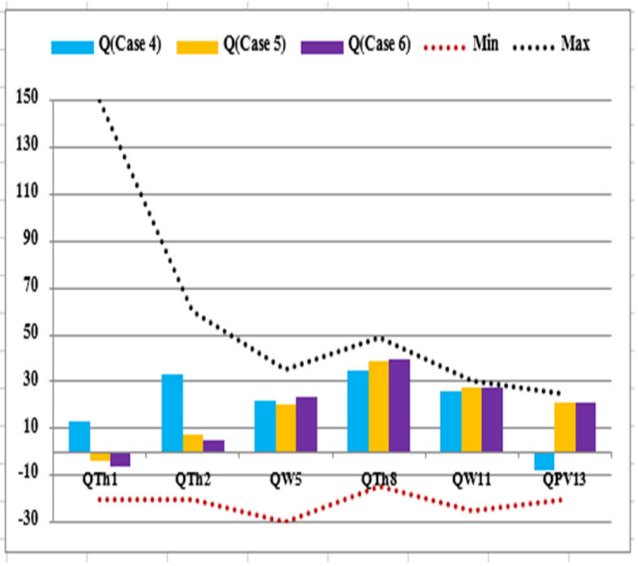

FIGURE 27. Schedule for reactive power from the generators for Cases 4, 5, and 6.

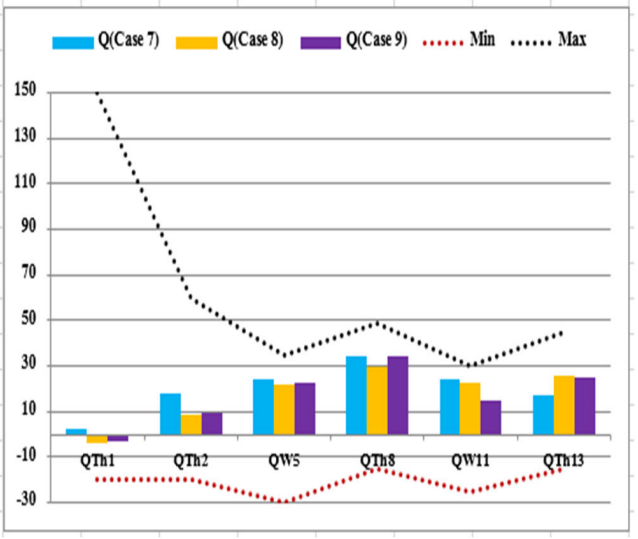

FIGURE 28. Schedule for reactive power from the generators for Cases 7, 8, and 9.

Tables (5-13), it becomes evident that the operation of all generators often operates at or near their limits for reactive power capability. Therefore, it is essential to pay attention to managing the reactive power restrictions when optimizing the technique. Proper constraint management strategies enable network components to operate close to their limits without exceeding them, offering an advantage in maintaining system stability.

V. CONCLUSION

In this study, the optimal power flow problem in a power system that includes solar PV farms, wind energy producers, and thermal generators has been successfully addressed. By minimizing the three distinct objective functions - total

generation cost, transmission losses, and gross cost - the study offers the most efficient generating schedules. The objective of minimizing overall generating costs encompasses reducing the expenses associated with traditional thermal generators, mitigating the risks associated with procuring wind and solar electricity from private owners, and minimizing the costs of conventional thermal generators. Additionally, in order to achieve cost-effective and environmentally friendly power supply solutions, new optimal approaches (CGO, RIME, OOA, and SMA) have been utilized to improve the power electrical network's quality by incorporating renewable energy resources and determining the optimal placement and size of FACTS devices. The results indicate that CGO outperforms other techniques in terms of its ability to handle complex OPF problems with a low convergence rate and minimal computational costs, making it the most effective metaheuristic technique. Future work can involve integrating energy storage systems into the optimal power flow framework to enhance the flexibility and reliability of the power system. Additionally, exploring advanced machine learning algorithms and artificial intelligence techniques for optimizing power flow in multi-energy systems could provide more accurate and computationally efficient solutions. This would contribute to the advancement of power system operation and planning, particularly in the context of renewable energy integration.

ACKNOWLEDGMENT

This project has received funding from the European Union's Horizon 2020 research and innovation programme under Marie Skłodowska-Curie grant agreement No. 801342 (Tecniospring INDUSTRY) and the Government of Catalonia's Agency for Business Competitiveness (ACCIÓ).

REFERENCES

[1] A. A. Mohamed, S. Kamel, M. H. Hassan, M. I. Mosaad, and M. Aljohani, "Optimal power flow analysis based on hybrid gradient-based optimizer with Moth–Flame optimization algorithm considering optimal placement and sizing of FACTS/wind power," *Mathematics*, vol. 10, no. 3, p. 361, Jan. 2022.

[2] A. A. Mohamed, S. Kamel, M. H. Hassan, and H. Zeinoddini-Meymand, "CAVOA: A chaotic optimization algorithm for optimal power flow with facts devices and stochastic wind power generation," *IET Gener., Transmiss. Distrib.*, vol. 18, no. 1, pp. 121–144, Jan. 2024.

[3] Y. M. Ammar, A. A. Elbaset, A. S. Adail, S. E. L. Araby, and A. A. Saleh, "A review on optimal UPFC device placement in electric power systems," *Kerntechnik*, vol. 87, no. 6, pp. 661–671, Dec. 2022.

[4] A. Mohamed, S. Mohamed, A. El-Gaafary, and M. Hemeida, "Optimal power-flow using moth swarm algorithm," *Electr. Power Syst. Res.*, vol. 142, pp. 190–206, Jan. 2017.

[5] A. Meng, C. Zeng, P. Wang, D. Chen, T. Zhou, X. Zheng, and H. Yin, "A high-performance crisscross search based grey wolf optimizer for solving optimal power flow problem," *Energy*, vol. 225, Jun. 2021, Art. no. 120211.

[6] D. Prasad and V. Mukherjee, "A novel symbiotic organisms search algorithm for optimal power flow of power system with FACTS devices," *Eng. Sci. Technol., Int. J.*, vol. 19, no. 1, pp. 79–89, Mar. 2016.

[7] M. El-Azab, W. A. Omran, S. F. Mekhamer, and H. E. A. Talaat, "Allocation of FACTS devices using a probabilistic multi-objective approach incorporating various sources of uncertainty and dynamic line rating," *IEEE Access*, vol. 8, pp. 167647–167664, 2020, doi: 10.1109/ACCESS.2020.3023744.

[8] P. P. Biswas, P. Arora, R. Mallipeddi, P. N. Suganthan, and B. K. Panigrahi, "Optimal placement and sizing of FACTS devices for optimal power flow in a wind power integrated electrical network," *Neural Comput. Appl.*, vol. 33, no. 12, pp. 6753–6774, Jun. 2021.

[9] S. Talatahari and M. Azizi, "Chaos game optimization: A novel metaheuristic algorithm," *Artif. Intell. Rev.*, vol. 54, no. 2, pp. 917–1004, Feb. 2021.

[10] M. Dehghani and P. Trojovský, "Osprey optimization algorithm: A new bio-inspired metaheuristic algorithm for solving engineering optimization problems," *Frontiers Mech. Eng.*, vol. 8, Jan. 2023, Art. no. 1126450, doi: 10.3389/fmech.2022.1126450.

[11] H. Su, D. Zhao, A. A. Heidari, L. Liu, X. Zhang, M. Mafarja, and H. Chen, "RIME: A physics-based optimization," *Neurocomputing*, vol. 532, pp. 183–214, May 2023.

[12] S. Li, H. Chen, M. Wang, A. A. Heidari, and S. Mirjalili, "Slime mould algorithm: A new method for stochastic optimization," *Future Gener. Comput. Syst.*, vol. 111, pp. 300–323, Oct. 2020.

[13] A. Sarwat, P. McCluskey, S. K. Mazumder, M. Russell, S. Roy, S. Tufail, S. Dharmasena, and A. Stevenson, "Reliability assessment of grid connected solar inverters in 1.4 MW PV plant from anomalous classified real field data," in *Proc. North Amer. Power Symp. (NAPS)*, Salt Lake City, UT, USA, Oct. 2022, pp. 1–6, doi: 10.1109/NAPS56150.2022.10012172.

[14] A. Debnath, S. Roy, T. O. Olowu, I. Parvez, and A. Sarwat, "A unified controller for hybrid PV-battery system with DC microgrid voltage regulation in grid-connected and islanding-mode," in *Proc. IEEE Ind. Appl. Soc. Annu. Meeting (IAS)*, Oct. 2022, pp. 1–6, doi: 10.1109/IAS54023.2022.9940125.

[15] T. Niknam, M. R. Narimani, and R. Azizipanah-Abarghooee, "A new hybrid algorithm for optimal power flow considering prohibited zones and valve point effect," *Energy Convers. Manag.*, vol. 58, pp. 197–206, Jun. 2012.

[16] A. S. Alghamdi, "Optimal power flow of renewable-integrated power systems using a Gaussian bare-bones levy-flight firefly algorithm," *Frontiers Energy Res.*, vol. 10, p. 697, May 2022.

[17] H. R. E. H. Bouchekara, A. E. Chaib, M. A. Abido, and R. A. El-Sehiemy, "Optimal power flow using an improved colliding bodies optimization algorithm," *Appl. Soft Comput.*, vol. 42, pp. 119–131, May 2016.

[18] M. Farhat, S. Kamel, A. M. Atallah, and B. Khan, "Optimal power flow solution based on jellyfish search optimization considering uncertainty of renewable energy sources," *IEEE Access*, vol. 9, pp. 100911–100933, 2021.

[19] M. H. Sulaiman and Z. Mustaffa, "Optimal power flow incorporating stochastic wind and solar generation by metaheuristic optimizers," *Microsyst. Technol.*, vol. 27, no. 9, pp. 3263–3277, Sep. 2021.

[20] N. Taleb, B. Bentouati, and S. Chettih, "Optimal power flow solutions incorporating stochastic solar power with the application grey wolf optimize," *J. Renew. Energy Sustain. Develop.*, vol. 3, no. 1, pp. 74–84, 2021.

[21] S. B. Pandya, J. Visumathi, M. Mahdal, T. K. Mahanta, and P. Jangir, "A novel MOGNDO algorithm for security-constrained optimal power flow problems," *Electronics*, vol. 11, no. 22, p. 3825, Nov. 2022.

[22] X. Weng, P. Xuan, A. A. Heidari, Z. Cai, H. Chen, R. F. Mansour, and M. Ragab, "A vertical and horizontal crossover sine cosine algorithm with pattern search for optimal power flow in power systems," *Energy*, vol. 271, May 2023, Art. no. 127000.

[23] P. P. Biswas, P. N. Suganthan, and G. A. J. Amaratunga, "Optimal power flow solutions incorporating stochastic wind and solar power," *Energy Convers. Manag.*, vol. 148, pp. 1194–1207, Sep. 2017.

[24] H. Xu, J. Nan, J. Feng, X. Deng, K. Sun, and H. Zhou, "Research on the impact of carbon tax on low-carbon economic dispatch," in *Proc. Annu. Conf. Power Syst. Automat. Chinese Universities*. Singapore: Springer, 2022, pp. 417–429.

[25] I. Marouani, T. Guesmi, H. Hadj Abdallah, B. M. Alshammari, K. Alqunun, A. S. Alshammari, and S. Rahmani, "Combined economic emission dispatch with and without consideration of PV and wind energy by using various optimization techniques: A review," *Energies*, vol. 15, no. 12, p. 4472, Jun. 2022.

[26] S. Mouassa, A. Alateeq, A. Alassaf, R. Bayindir, I. Alsaleh, and F. Jurado, "Optimal power flow analysis with renewable energy resource uncertainty using dwarf mongoose optimizer: Case of ADRAR isolated electrical network," *IEEE Access*, vol. 12, pp. 10202–10218, 2024.

[27] M. J. Morshed and A. Fekih, "A fault-tolerant control paradigm for microgrid-connected wind energy systems," *IEEE Syst. J.*, vol. 12, no. 1, pp. 360–372, Mar. 2018.

[28] *Wind Turbines—Part 1: Design Requirements*, Standard IEC61400 61400-1, 2005, p. 177.
[29] O. Alsac and B. Stott, "Optimal load flow with steady-state security," *IEEE Trans. Power App. Syst.* , vol. PAS-93, no. 3, pp. 745–751, May 1974.
[30] R. D. Zimmerman and C. E. Murillo-Sánchez, "Matpower (version 7.0) [software]," Tech. Rep., Version 7.0, Jun. 2019, doi: 10.5281/zenodo.3251119.

AMAL AMIN MOHAMED received the M.Sc. degree from the Faculty of Engineering, Aswan University, Egypt, in 2020. She is currently pursuing the Ph.D. degree with the Department of Electrical Engineering, Aswan Faculty of Engineering, Aswan University. Her research activities include power system modeling, analysis, and optimization.

SALAH KAMEL received the international Ph.D. degree from Jaen University, Spain (Main), and Aalborg University, Denmark (Host), in January 2014. His research interests include power system analysis and optimization, smart grids, and renewable energy systems.

MOHAMED H. HASSAN received the B.Sc. degree in electrical engineering from Minia University, Egypt, in 2011, the M.Sc. degree from Cairo University, Egypt, in 2018, and the joint Ph.D. degree supervision between Aswan University, Egypt, and the University of Jaen, Spain, in 2022. His research interests include optimization techniques and smart grids.

JOSÉ LUIS DOMÍNGUEZ-GARCÍA (Senior Member, IEEE) received the B.S. and M.S. degrees in industrial engineering in 2009 and the Ph.D. degree in electrical engineering in 2013. He was a Visiting Researcher with the Institute of Energy, Cardiff University, in 2011; the University of Strathclyde, Glasgow, in 2016; and Huddersfield University, U.K., in 2018. His work deals with the grid integration of renewable energy sources, smart grids, and microgrids.